JOURNAL OF NEUROTRAUMA 28:2245–2262 (November 2011)

DOI: 10.1089/neu.2010.1499

Rate of Neurodegeneration in the Mouse Controlled Cortical Impact Model Is Influenced by Impactor Tip Shape: Implications for Mechanistic and Therapeutic Studies

Jennifer M. Pleasant,[1,*] Shaun W. Carlson,[1,*] Haojie Mao,[3] Stephen W. Scheff,[2] King H. Yang,[3] and Kathryn E. Saatman[1]

Abstract

Controlled cortical impact (CCI), one of the most common models of traumatic brain injury, is being increasingly used with mice for exploration of cell injury mechanisms and pre-clinical evaluation of therapeutic strategies. Although CCI brain injury was originally effected using an impactor with a rounded tip, the majority of studies with mouse CCI use a flat or beveled tip. Recent finite element modeling analyses demonstrate that tip geometry is a significant determinant of predicted cortical tissue strains in rat CCI, and that cell death is proportional to predicted tissue strains. In the current study, a three-dimensional finite element model of a C57BL/6J mouse brain predicted higher maximum principal strains during a simulated 1.0-mm, 3.5-m/s CCI injury with a flat tip when compared to a rounded tip. Consistent with this prediction, experimental CCI with a flat-tip impactor resulted in greater acute cortical hemorrhage and neuron loss in adult male C57BL/6J mice. The amount of neocortical tissue damage was equivalent for the two tip geometries at 9 days following injury, but the rate of neocortical neurodegeneration was markedly slower following CCI with a rounded-tip impactor, with damage reaching a plateau after 24 h as opposed to after 4 h for the flat tip. The flat-tip impactor was associated in general with more regional hippocampal neurodegeneration, especially at early time points such as 4 h. Impactor tip geometry did not have a notable effect on blood–brain barrier breakdown, traumatic axonal injury, or motor and cognitive dysfunction. Execution of CCI injury with a rounded-tip impactor is posited to provide a substantially enhanced temporal window for the study of cellular injury mechanisms and therapeutic intervention while maintaining critical aspects of the pathophysiological response to contusion brain injury.

Key words: axonal injury; behavior; contusion; finite element modeling; neuronal death; traumatic brain injury

Introduction

The annual incidence of traumatic brain injury (TBI) is estimated at more than 1.5 million people in the United States alone, with many cases of mild TBI probably unreported. Although numerous clinical trials have been conducted for moderate-to-severe TBI, no therapeutic intervention has proven effective in improving functional outcome (Maas et al., 2010; Narayan et al., 2002). The difficulty in establishing an effective pharmacological treatment approach is thought to be related, in part, to the heterogeneity of TBI (Maas et al., 1999; Saatman et al., 2008). At a cellular level, complexity arises from multiple, interacting secondary injury cascades that, over time, amplify primary damage inflicted during the traumatic insult. At a tissue level, TBI is heterogeneous in that it comprises multiple pathoanatomical types of injury, such as contusion, diffuse axonal injury, and hematoma, which probably involve different combinations of primary damage and secondary mediators. To overcome this challenge, treatment approaches tailored to a selected pathoanatomical injury type may be utilized in future clinical trials for TBI. Contusion injury is well suited to this targeted therapy approach for several reasons. Contusion represents a common type of TBI that can be diagnosed using standard radiological imaging (Alahmadi et al., 2010; Maas et al., 2005; Marshall et al., 1992). Furthermore, animal models of contusion injury are

[1]Spinal Cord and Brain Injury Research Center and Department of Physiology, and [2]Sanders-Brown Center on Aging and Department of Anatomy and Neurobiology, University of Kentucky College of Medicine, Lexington, Kentucky.
[3]Bioengineering Center, Wayne State University, Detroit, Michigan.
*These authors contributed equally to this work.

widely used for identification of injury mechanisms and the pre-clinical evaluation of therapeutic interventions.

The controlled cortical impact (CCI) model is one of the most commonly used models of contusion TBI. The CCI model utilizes a metal impactor rod to transiently and rapidly deform the cortex exposed via a craniotomy. The model was originally developed for use in ferrets (Lighthall, 1988), but was subsequently adapted for rats (Dixon et al., 1991) and mice (Smith et al., 1995). The use of CCI brain injury in mice has dramatically increased over the past 15 years as a result of greater reliance on transgenic and knockout mice for the study of cellular mechanisms, and the cost- effectiveness of mice for therapeutic testing. In both mice (Fox et al., 1998; Hall et al., 2005; Hannay et al., 1999; Saatman et al., 2006; Smith et al., 1995) and rats (Dixon et al., 1991; Goodman et al., 1994; Hamm et al., 1992; Hicks et al., 1997; Scheff et al., 1997; Sutton et al., 1993), experimental CCI reproduces important features of human contusion TBI such as neocortical and hippocampal cell loss by necrosis and apoptosis, axonal injury, blood–brain barrier (BBB) breakdown, and cognitive and motor deficits. In the process of characterizing the CCI model, a number of laboratories have demonstrated that changing the depth or velocity of impact or the number of craniotomies influences the location and severity of injury (Dixon et al., 1991; Fox et al., 1998; Goodman et al., 1994; Hannay et al., 1999; Meaney et al., 1994; Saatman et al., 2006; Sutton et al., 1993).

In contrast, the effects of the shape of the impactor tip on the histopathological or behavioral response to CCI brain injury have not been systematically investigated. Interestingly, the shape of the impactor tip is frequently not described in the methodology of published CCI studies. The model was originally developed with a rounded-tip impactor (Lighthall 1988). However, in mouse CCI studies that do describe the impactor, nearly all describe the tip as "flat" or "beveled flat", that is, a flat surface where the impactor contacts the exposed brain tissue (Dennis et al., 2009; Fox et al., 1998; Sandhir and Berman, 2010; Smith et al., 1995; Thompson et al., 2006; Whalen et al., 2008; Xiong et al., 2005). We recently demonstrated that, after impact depth, tip geometry (flat versus rounded) was the most important parameter in estimating tissue strains and predicting cortical contusion volume in a rat finite element simulation, exceeding the influence of impact velocity, tip diameter, or number of craniotomies (Mao et al., 2010b). Simulations demonstrated that impact with a flat tip resulted in high tissue strains localized at the impactor rim, whereas strains produced by impact with a rounded (spherical) tip were more radially distributed.

In our experience, the use of a flat-tip impactor frequently resulted in very rapid cortical neuron death, extensive cortical hemorrhage and distortion, and sometimes even cortical tissue tearing in mice subjected to moderate or severe CCI. We reasoned that by using a hemispheric (rounded) tip, we could decrease tensile/shear strains at the edges of the impactor as it penetrated the cortical tissue, resulting in less ablative primary cellular damage and a more gradual progression of neuronal death, thereby enhancing the fidelity of the model to human closed head contusion injury.

To test this hypothesis, we utilized a finite element modeling approach to visualize and compare the patterns of maximum principal (tensile) strains produced by deformation of the mouse cortex with either a flat or rounded-tip impactor. We then compared the histological damage and the time course for neocortical contusion formation from 1 h to 9 days after a 1.0-mm-depth impact with these two tips. To provide a comprehensive evaluation of the effects of modulating the tip shape, we also evaluated other important features of CCI brain injury such as regional hippocampal neurodegeneration, BBB breakdown, axonal injury, and neurobehavioral deficits. Our data suggest that cortical impact with either a flat or rounded-tip impactor results in equivalent neocortical cell death at 9 days after injury, similar patterns of BBB breakdown and axonal injury, and equivalent neurobehavioral impairment and recovery. Importantly, however, impact with a rounded-tip impactor reduced cortical tissue strains at the impactor edges, slowed the progression of cortical cell death, and reduced the extent of acute hippocampal neurodegeneration. These findings have important implications for investigations of cellular mechanisms of damage and testing of therapeutic interventions for contusion TBI.

Methods

Finite element mouse brain model development and CCI simulations

Considering anatomical similarity between rat and mouse brains, a previously developed rat brain finite element model (Mao et al., 2006) was used as the basis for generating a finite element mouse brain model. The geometry used for developing the mouse brain model was taken from a comprehensive three-dimensional C57BL/6J mouse brain atlas reported by Ma and colleagues (2005). Ma and colleagues acquired microscopy images from 10 adult male (12–14 weeks, weight range 25–30 g) C57BL/6J mice at a 47-μm isotropic resolution using a 17.6-T magnetic resonance imaging device. The "minimum deformation atlas", a representation of the average structural shape of the 10 mice, was adopted here for developing a mouse brain model. The images were imported to an imaging processing software MIMICS 12 (Materialise, Leuven, Belgium) to segment the outer surface of the brain, exterior surfaces of the white matter, and ventricles. The Meshworks 5.0/Morpher (DEP, Troy, MI) was then used to morph the exterior meshes of the rat brain model to the outer surface of the mouse brain. After that, the white matter and ventricles were adjusted according to the mouse brain anatomy. The morphed mouse brain model, consisting of the cerebrum, cerebellum, corpus callosum, internal and external capsules, lateral ventricles, olfactory bulb, brainstem, and part of spinal cord, has a total of 258,428 brick elements with a typical spatial resolution of 150 μm (Fig. 1). To the best of the authors' knowledge, material properties regarding mouse brain were not reported in the literature. Therefore, the mouse brain material properties were defined based on combined *in vitro* and *in situ* indentation tests of non-preconditioned adult rat brains reported by Gefen and associates (2003) using a linear viscoelastic material law (LS-DYNA Material Type 61, Livermore Software Technology Corporation, Livermore, CA). For the gray matter, cerebellum, and brainstem, a short-term shear modulus of 1.72 kPa and a long-term shear modulus of 0.51 kPa were assumed. For the white matter, a short-term modulus of 1.2 kPa and a long-term modulus of 0.36 kPa were assumed. A decay constant of 20 ms was assumed for both the white and gray matter. Additionally, the ventricles were assumed to have a short-term modulus of 1 kPa and a long-term modulus of 0.3 kPa while the corresponding pa-

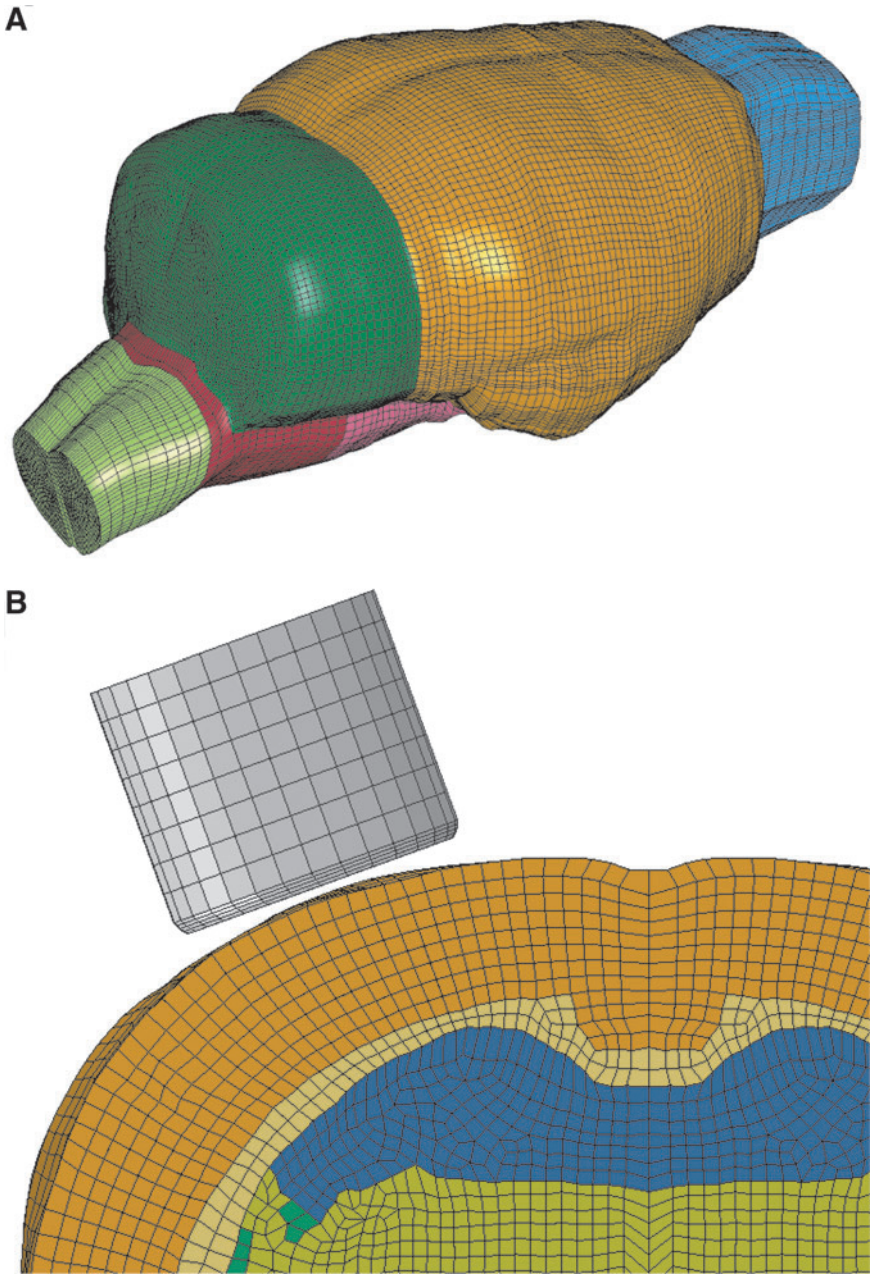

FIG. 1. Finite element model of mouse brain and impactor. **(A)** Isometric view of the three-dimensional finite element model of the mouse brain utilized for simulation of CCI brain injury. **(B)** Cross-sectional view of the ipsilateral dorsal quadrant of the brain model illustrating interior structures, the mesh size, and the position of the impactor.

rameters for the spinal cord were assumed to be 3.1 and 0.92 kPa, respectively. For the membranes, linear elastic material properties were assumed with a Young's modulus of 12.5 MPa for the pia-arachnoid complex (Jin et al., 2006) and 31.5 MPa for dura (Galford and McElhaney, 1970).

Two CCI scenarios using a 2.5-mm diameter, flat tip and a 3.0-mm diameter, hemispherical (rounded) tip impactor, identical to experimental conditions, were simulated. The hemispherical tip was designed to be slightly larger in diameter to partially offset the decrease in tip volume caused by rounding of the tip. A 4.5-mm diameter craniotomy, centered at −2.5-mm bregma and 2.75 mm lateral to the midline, was removed from the mouse skull model. The impactor compressed the exposed dura for up to 1.0 mm at a velocity of 3.51 m/s, the mean value calculated from experimental records. The simulation duration was set as 2 ms and simulation results were plotted at every 0.02 ms. The depth of impact was set at 1.0 mm for both impactors to mimic commonly used experimental protocols, and to control for the variable most critical in determining tissue strains in the CCI model (Mao et al., 2010b).

Animals and surgical procedures

Adult male C57BL/6J mice (The Jackson Laboratory, Bar Harbor, ME), weighing 22–32 g, were housed in a room with a

14:10 light:dark photoperiod. Mice were given food and water *ad libitum*. All animal experiments and procedures were in accordance with the National Institutes of Health Guide for the Care and Use of Laboratory Animals and were approved by the University of Kentucky Institutional Animal Care and Use Committee.

Mice were anesthetized using 2.5% isoflurane, their heads were shaved, and they were placed in a stereotaxic frame (Kopf, Tujunga, CA) where they were maintained on isoflurane delivered by a nose cone. A midline incision was made to expose the skull, and a 4.5-mm craniotomy was made centered at −2.5mm bregma and 2.75 mm lateral to midline over the left hemisphere. Mice were subjected to CCI injury at a 1.0-mm impact depth and a nominal velocity of 3.5 m/s. The CCI impactor device (TBI-0310 Impactor, Precision Systems and Instrumentation, Fairfax Station, VA) uses a computer controlled pneumatically driven piston to rapidly impact the brain. This system has a sensitive mechanism for detecting the cortical surface after which the impactor is automatically repositioned for a user-determined impact depth. Mice were randomized for injury with either a flat tip or rounded-tip impactor (Fig. 2A). After injury, a cranioplast was placed over the exposed brain. The mice were sutured and placed on a heating pad to maintain normal body temperature until they were fully awake, after which they were returned to their home cages.

Tissue preparation

At 1, 4, 12, or 24 h, or 9 days, ($n=5$ injured with a flat-tip impactor, $n=5$ injured with a rounded-tip impactor per time point) mice were anesthetized with 65 mg/kg sodium

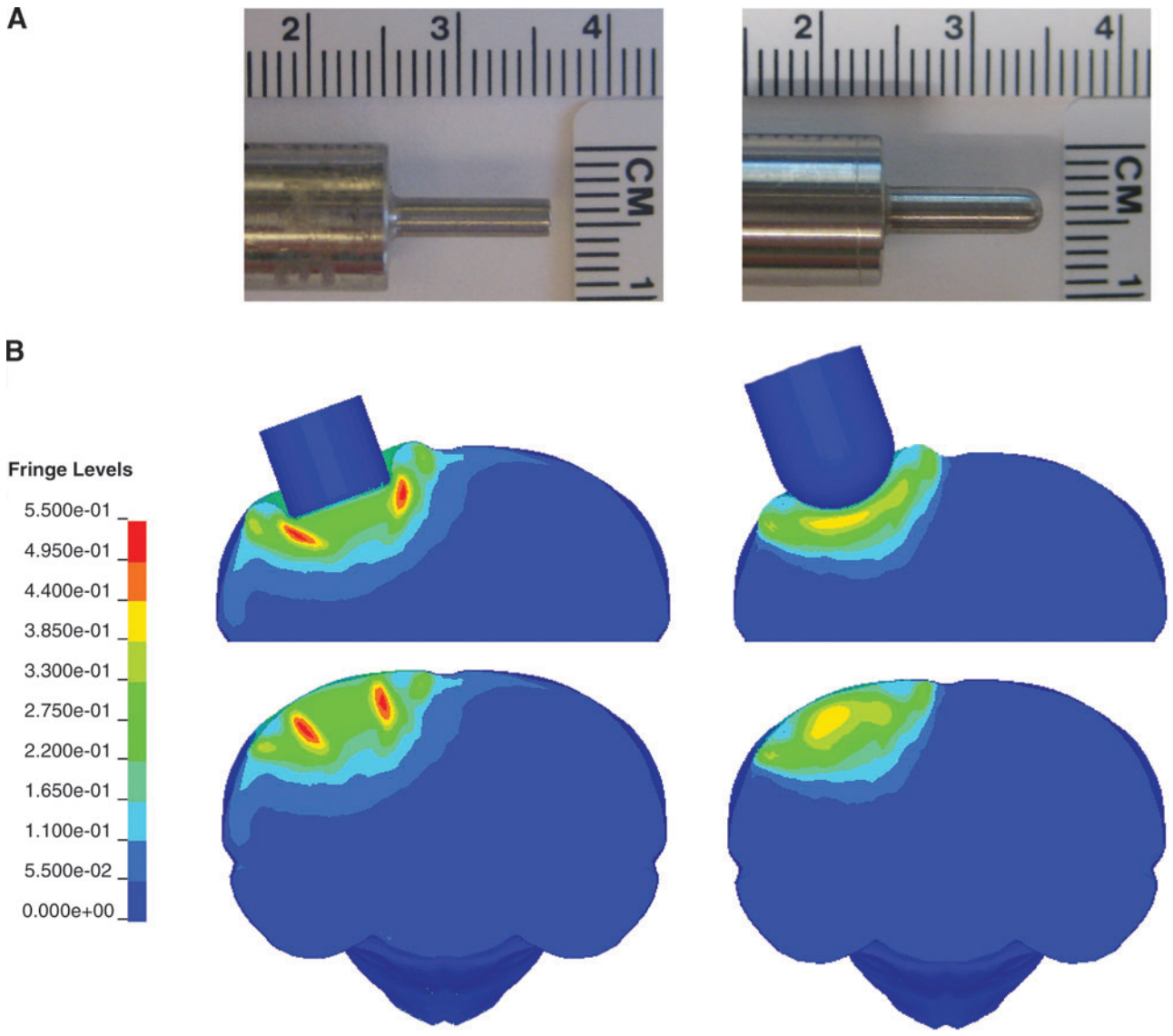

FIG. 2. Effect of impactor shape on brain tissue strains. **(A)** Animals received CCI with either a flat tip (left) or rounded tip (right) metal impactor rod. **(B)** The impactor tip shapes were reproduced for the finite element simulations shown here, illustrating the maximum principal (tensile) strain contours in a coronal section through the impact center at an impact depth of 1.0 mm. Contours are shown with the tip in place (upper maps) and with strains mapped to the undeformed brain (lower maps). The fringe levels indicate the strain levels (0 to 0.5500) represented by colors in each contour map.

pentobarbital through an intraperitoneal injection. Mice were then intracardially perfused with heparinized saline followed by 10% buffered formalin, and decapitated. After 24 h of fixation in 10% buffered formalin, the brains were removed from the skull, post-fixed for 24 h, cryoprotected in 30% sucrose, and quickly frozen in −30°C isopentane. Coronal 40-μm sections were cut using a freezing sliding microtome (Dolby-Jamison, Pottstown, PA).

Cortical contusion volume

Brain sections selected at 400-μm intervals between 0 and −3.5 mm bregma (Paxinos and Franklin, 2001) were stained for Nissl substance using 2.5% cresyl violet and mounted onto slides. Existing methods were modified slightly to quantify the neocortical area containing surviving neurons (Royo et al., 2006; Saatman et al., 2006). Sections were viewed using a light microscope (BH2, Olympus America Inc., Melville, NY) equipped with an automated stage and camera. On a live image, the neocortices of the contralateral and ipsilateral hemispheres were separately outlined using a tracing tool (BIOQUANT Life Science version 8.40.20, BIOQUANT Image Analysis Corporation, Nashville, TN), alternating between 2 x and 10 x magnification to evaluate the boundaries of the neocortex as well as cellular staining and morphology. Only areas containing Nissl-stained cells with presumed neuronal morphology were outlined, thereby excluding areas of necrotic tissue. Contusion area was calculated as the difference between the contralateral and spared ipsilateral neocortical areas. The contusion volume was obtained using Cavalieri's principle, integrating over the inter-section distance, and is expressed as a percentage of the contralateral neocortical volume to control for any potential variation in tissue shrinkage during fixation and freezing.

Regional hippocampal neurodegeneration

Fluorojade-B staining (Millipore Co., Billerica, MA) for degenerating neurons (Schmued et al., 1997) has been used to quantify trauma-induced hippocampal neuron death (Anderson et al., 2005; Dennis et al., 2009). Brain sections containing hippocampus were selected every 800 μm between bregma levels −1.06 mm and −3.5 mm (Paxinos and Franklin, 2001) from mice that survived 1, 4, 12, and 24 h. After rinsing in Tris-buffered saline (TBS), sections were immersed in diaminobenzidine (DAB) (Vector Laboratories, Inc., Burlingame, CA) for 5 min to provide a substrate for endogenous peroxidases and to eliminate autofluorescence from parenchymal hemorrhage. Sections were then mounted onto slides, warmed at 40–45°C for 30 min, and kept at room temperature overnight. On day 2, slides were immersed sequentially in 1% NaOH in 80% EtOH, 70% EtOH, and ddH_2O. Sections were placed in a 0.06% potassium permanganate solution for 10 min and rinsed in ddH_2O, before staining 10 min with 0.0001% Fluorojade-B in 0.1% acetic acid. Slides were then rinsed in ddH_2O, dried on a slide warmer at 50°C, immersed in Xylenes (Fisher Scientific, Fair Lawns, NJ), and coverslipped in Cytoseal XYL (Richard-Allan Scientific, Kalamazoo, MI). For quantification, Fluorojade-positive neurons were counted separately within the dentate gyrus, CA3/CA3c, and CA1 of the ipsilateral hippocampus in three sections centered within the impact site. Counting was performed at 20 x under a fluorescence microscope equipped with an FITC filter (AX80, Olympus America) by an individual blinded to the injury conditions of each animal.

Immunohistochemistry

Immunoglobulin (IgG). Free-floating sections, adjacent to those used for both Nissl and Fluorojade-B staining, were used for immunohistochemical analysis of IgG extravasation, indicative of BBB breakdown. Tissue was rinsed in TBS and treated with a 3% H_2O_2 solution to quench endogenous peroxidases before blocking nonspecific binding sites with 5% normal horse serum (NHS). Biotinylated donkey anti-mouse IgG antibody (1:1000, Jackson Immuno Research) was applied overnight at 4°C. Negative control sections were incubated in diluent without primary antibody. On day 2, the tissue was rinsed in TBS and incubated in an avidin-biotin complex (AB Elite Kit, Vector Laboratories) and reacted with DAB.

Amyloid precursor protein. Immunohistochemical detection of amyloid precursor protein (APP) accumulation in axons is a commonly used marker for acute traumatic axonal injury (Sheriff et al., 1994; Stone et al., 2000). Sections were rinsed in TBS and placed in 10M citric acid at 65°C for 15 min for antigen retrieval. Tissue was then washed in TBS, blocked in 5% NHS in 0.1% Triton X-100 and incubated overnight at 4°C in 1:500 anti-C-terminal APP (Cat # 51-2700, Invitrogen, Carlsbad, CA). Following incubation in 1:1000 biotinylated donkey anti-rabbit IgG secondary antibody, endogenous peroxidases were blocked using 0.9% H_2O_2 in 50% methanol. Tissue was then rinsed and incubated in avidin-biotin complex. Reaction product was visualized using DAB as a substrate.

Behavioral testing

Following CCI injury, mice to be used for analysis of tissue damage at 9 days post-injury ($n = 5$/impactor tip) were subjected to behavior tests at several time points to assess their level of motor and cognitive function. All behavior tests were performed by a blinded evaluator.

Neurological severity score (NSS). An NSS, adapted from Tsenter and associates (2008), was assessed at 1 h and 1, 2, 5 and 7 days. NSS is a 14-point ordinal scale with 14 representing normal motor function. Mice were scored as they traversed, in sequence, 3, 2, 1, and 0.5 cm wide Plexiglas beams (60 cm long) and a 0.5 cm diameter wooden rod (60 cm long). The beams and rod were elevated 47 cm above the table top. Mice were acclimated to walking across the beams and rod 24 h before injury. Mice were allowed up to 30 sec to cross the beams and rod during both acclimation and testing. Each beam had a maximum of three points; three points were given for successfully crossing the beam with normal forelimb and hindlimb position, two points were given for successfully crossing the beam despite either a forelimb or hindlimb hanging from the beam, and one point was given for crossing the beam despite inverting underneath the beam one or more times. If a mouse became inverted on the beam, it was righted and allowed to continue across. The mouse scored a 0 if it did not cross the beam in the allotted time or if it fell off the beam. For the wooden rod, there was a maximum of two points. A mouse received two points for successfully crossing the rod and one point was given for crossing despite inverting more

than three times. A mouse received a 0 if it did not traverse or fell off of the rod.

Neuroscore. Neurological motor function was also assessed at 1, 2, 5, and 7 days post-injury, using a 12-point neuroscore evaluation. The neuroscore test was performed as previously described (Scherbel et al., 1999) with slight modifications. The neuroscore evaluation consisted of three tests: the grid walk (two points), forelimb and hindlimb flexion tests (three points each), and lateral pulsion (four points). For the grid walk, mice were placed upon a wire grate with bars spaced 1.5 cm apart positioned 20 cm above a table. One point was deducted if either a front or hind paw slipped through the grate without immediate recovery during 60 sec of free exploration. Mice scored a 0 if they had both forelimb and hindlimb slips. In the flexion tests, limb coordination and grip strength were evaluated as mice were suspended by their tail over a metal rung cage top and lowered to allow them to grasp the cage bars with both forelimbs. One point was deducted from the forelimb score if the mouse had low grip strength, crossed its forelimbs, or had excessive hyperactivity. For the hindlimb score, abnormal limb extension or toe splaying each resulted in a one point deduction, whereas three points were deducted if the mouse curled its hindlimb up to its body. For the lateral pulsion test, mice were pushed four times from left to right across a ribbed plastic mat at increasing speeds. Four points were deducted for rolling over on the first trial, three points were deducted for rolling over on the second trial, two points were deducted for rolling over on the third trial, and one point was deducted for rolling over on the fourth trial. If the mouse did not roll over on any of the four trials, it received four points.

Morris water maze (MWM) cognitive test. Learning ability was evaluated on days 7–9 post-injury using a paradigm similar to those widely utilized in models of rodent TBI (Hamm et al., 1992; Prins and Hovda, 2001; Saatman et al., 1997). A 1-m diameter MWM was filled with 19–21°C water containing a nontoxic white paint (Rich Art Co., Northvale, NJ) to hide a 6.3-cm-diameter platform that was submerged 0.5 cm below the surface of the water. Mice were released into the water from one of four different starting points (North, East, South, or West quadrant) and their latency to locate the platform (located in the West quadrant) using large visual cues placed on the walls outside the tank was recorded. Mice were tested in sets of four trials per day over 3 consecutive days. If the mouse did not find the platform within the allotted 70 sec trial time, it was placed onto the platform for 5 sec, then returned to a heated cage. Swimming trials were monitored using an overhead video camera and tracking software (EZ-Video version 5.51DV, Accuscan Instruments Inc., Columbus, OH).

Statistical analysis

All data are presented as means and standard deviation. Contusion volumes were compared using a two-way ANOVA. Fluorojade-positive cell counts were analyzed using a two-way ANOVA for each hippocampal subfield. MWM training latencies, neuroscore and NSS motor function tests were analyzed using a repeated measures one-way ANOVA. In all cases, Neuman-Keuls post-hoc *t*-tests were performed when appropriate. A value of $p < 0.05$ was considered statistically significant.

Results

Finite element simulation of cortical impact injury

CCI brain injury at a 1.0-mm depth of impact was simulated for a flat-tip impactor and a rounded-tip impactor (Fig. 2A). Principal strain contours immediately after the maximum dural compression was reached are illustrated in Figure 2B. The peak maximum principal strains resulting from impact with a flat tip were ≥49.5–55.0%. In contrast, impact with a rounded tip generated lower peak maximum principal strains, in the range of 38.5–44.0%. In addition, the largest strains induced by the flat-tip impactor were highly localized along the impactor rim, while there were no such concentrations or "edge effects" observed for the rounded-tip impactor (Fig. 2B). The edge effect of the flat-tip impactor is also clearly evident in strain profiles illustrating the peak maximum principal strain as a function of element location along a lateral to medial cortical arc (Fig. 3), where element no.16 represents the position of the center of either the flat tip or rounded-tip impactor. At cortical layers 3 and 5, for example, impact with the flat tip induced strains at the impactor rim which were almost 100% higher than the strains beneath the impactor center. In contrast, the rounded tip produced more uniform strain distributions beneath the impactor. The difference between rounded tip and flat tip induced strains was less pronounced at the cortical surface (layer 1), where the highest strains were induced as a result of tissue protrusion between the impactor and the edge of the craniotomy. Strain elevations as a result of tissue protrusion (labeled A in Fig. 3) decreased as a function of cortical depth and were essentially eliminated by layer 7. In the hippocampal region, the peak maximum principal strain was 24.8% for the rounded tip group and 30.1% for flat tip group.

Histological damage in Nissl-stained brain sections

Histological analyses of cortical tissue damage using Nissl staining revealed that injury with a flat-tip impactor resulted in more pronounced initial tissue disruption and more rapid cell death when compared to impact with a rounded-tip impactor. Even though cell loss progressed at different rates, neocortical tissue damage was ultimately equivalent.

At 1 h post-injury, brains injured by the flat-tip impactor exhibited marked cortical swelling associated with extrusion at the craniotomy site (Fig. 4A). Hemorrhage and neuron loss was observed where cortical tissue strains were predicted to be maximal, at the periphery of the impactor. Hemorrhage was also frequently found at the interface of the cortex and the subcortical white matter. In most animals injured with the flat tip (3/5), hippocampal distortion and hemorrhage were prominent. In contrast, 1 h after injury with a rounded-tip impactor, brains exhibited no overt loss of Nissl staining, only mild-to-moderate cortical swelling, and minimal hemorrhage, typically along the cortical surface (Fig. 4B). The ipsilateral hippocampus was not distorted, and no hemorrhage was present.

At 4 h after injury with a flat-tip impactor, extensive neocortical cell death compromised tissue integrity (Fig. 4C), and began to result in tissue loss during the cutting and mounting

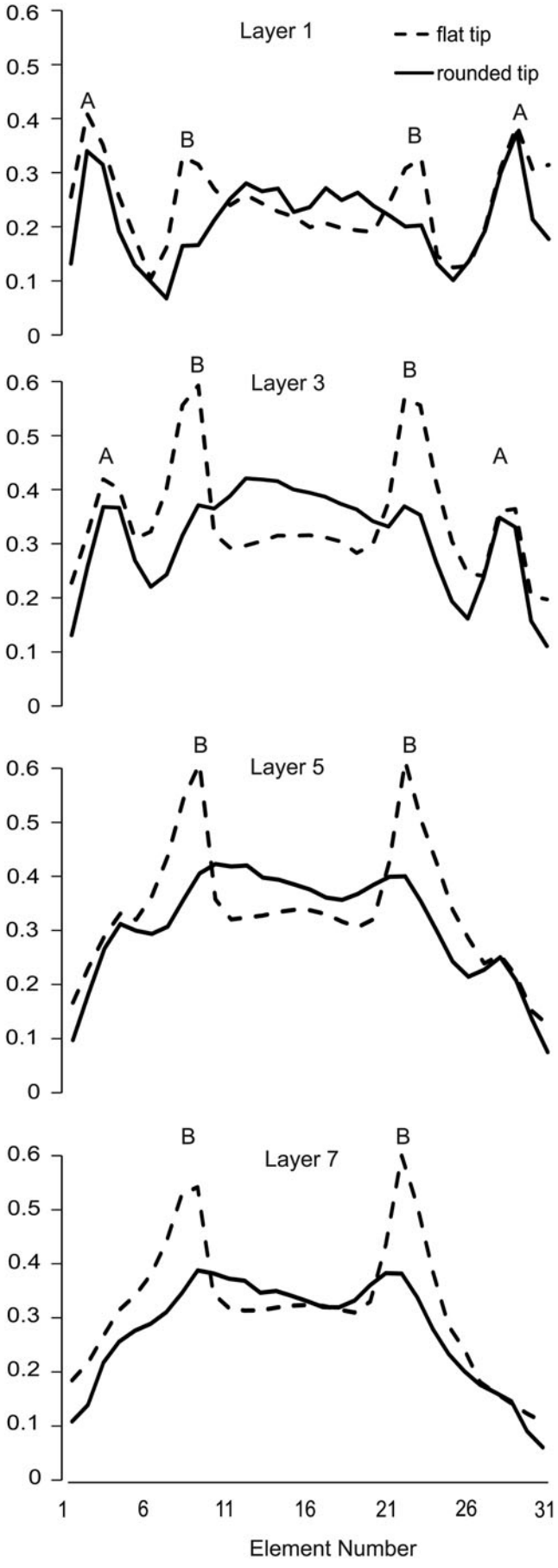

procedures. By 12 h, a cortical cavity or "lesion" was well formed (Fig. 4E). At 4 and 12 h, hippocampal hemorrhage (6/10) and distortion (9/10) were still prominent. After injury with a rounded-tip impactor, the contused neocortex exhibited mild-to-moderate swelling, mild intraparenchymal hemorrhage, and progressive loss of Nissl staining intensity from 4 to 12 h (Fig. 4D, F). The subcortical white matter tract was intact but exhibited some disruption and hemorrhage. No hippocampal hemorrhage was observed at 4 or 12 h after injury with a rounded- tip impactor, although distortion of the hippocampal formation was evident by 12 h.

By 1 and 9 days post-injury, histological damage in Nissl-stained brain sections from mice injured with either a flat and rounded-tip impactor appeared much more similar than at earlier time points. Both impactors resulted in the formation of a large cortical cavity by 1 day, with evidence of intraparenchymal hemorrhage surrounding the cavity (Fig. 4G, H). In both groups, the cortical cavity was lined by reactive glia by 9 days (Fig. 4I, J). As with the flat-tip impactor, the rounded-tip impactor produced subcortical white matter disconnection and degeneration in nearly all mice (9/10) at 1 and 9 days post-injury. Delayed hippocampal hemorrhage was noted at 1 day after rounded tip impact (3/5), whereas hemorrhage was not typical at 1 day after injury with a flat-tip impactor and was not observed at 9 days post-injury in either group.

Differences in gross histological responses to injury using a flat tip versus a rounded-tip impactor (described previously) were underscored by qualitative analysis of neocortical neuron morphology. As early as 1 h after injury with a flat-tip impactor, neocortical Nissl staining was diminished in intensity, and scattered cell loss and shrinkage was evident through all neocortical layers (Fig. 5A) when compared to uninjured tissue (Fig. 5E). Neurons in the neocortex injured by the rounded-tip impactor were pyknotic, but normal appearing in size, density, and Nissl intensity (Fig. 5B). At 4 h after injury with a flat-tip impactor, neocortical neuronal damage had progressed substantially, with few identifiable neurons visible in the contusion site (Fig. 5C). In the neocortex of mice injured with a rounded tip, Nissl-stained cells with neuronal morphology were still clearly detectable at 4 h (Fig. 5D), although pyknosis and loss of Nissl intensity was greater than at 1h. The extent of neuronal damage was far less than that induced at 4 h by a flat-tip impactor (compare Fig. 5C and D). Neuronal damage had increased by 12 h after impact with a rounded tip (Fig. 5F), with marked loss of Nissl staining comparable to that observed 4 h after injury with the flat-tip impactor (Fig. 5C).

FIG. 3. Strain profile as a function of cortical depth and tip geometry. The peak maximum principal strain at any time during the impact is plotted for 31 elements along a lateral to medial cortical arc, or cortical layer, in the finite element model. The model consists of eight cortical layers (see Figure 1B), with the cortical surface designated as Layer 1, and the deepest layer adjacent to the subcortical white matter designated as Layer 8. Element number 16 corresponds to the center of the impactor and craniotomy. Strain peaks labeled 'A' correspond to regions of tissue protrusion between the impactor and the craniotomy edge. Strain peaks labeled 'B' correspond to the edge effects created by the flat-tip impactor.

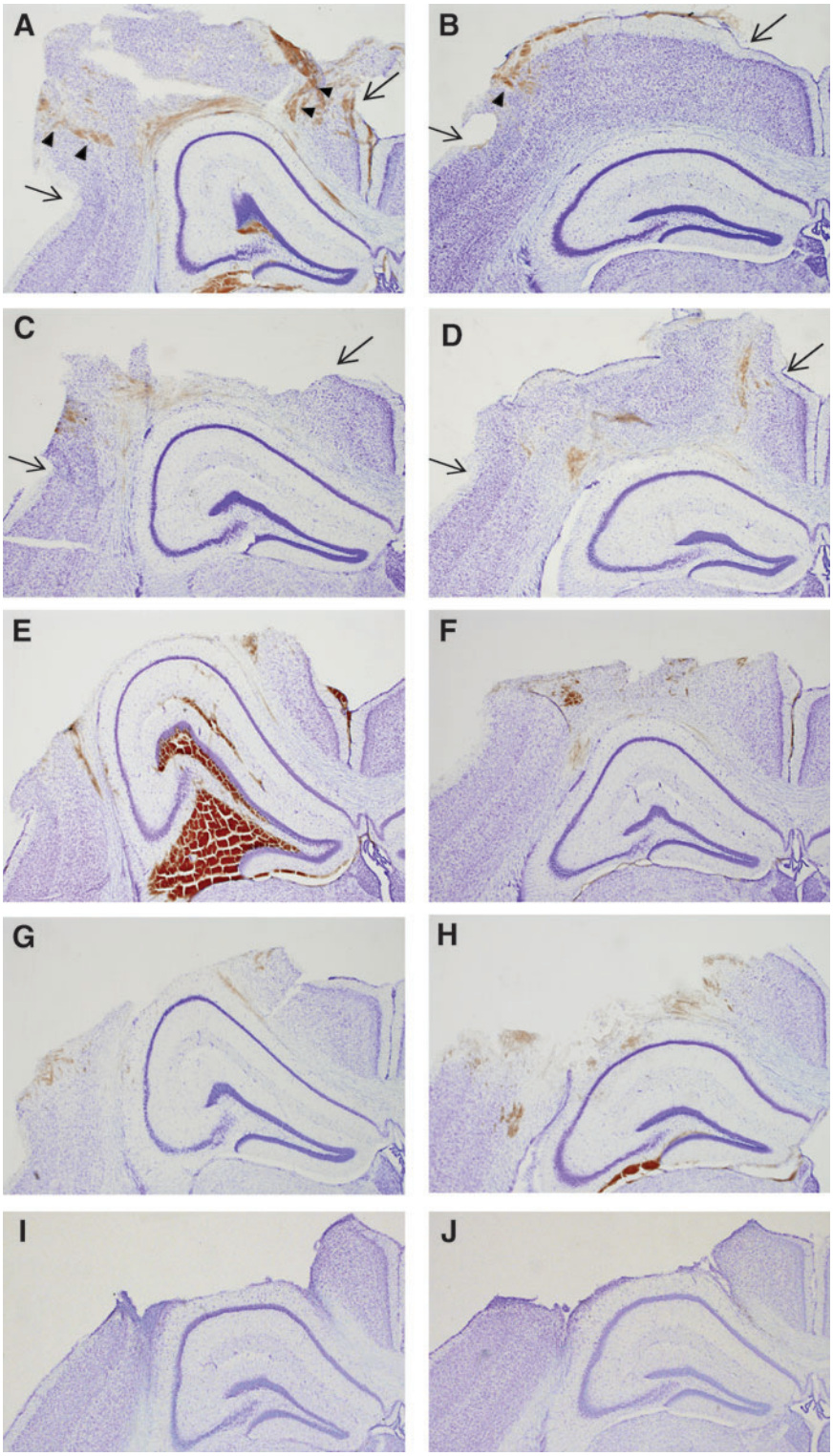

FIG. 4. Temporal progression of histological damage created by a flat-tip versus a rounded-tip CCI impactor. Images are shown of the ipsilateral neocortex and hippocampus of Nissl-stained coronal sections taken at the epicenter of the impact at 1 h **(A, B)**, 4 h **(C, D)**, 12 h **(E, F)**, 24 h **(G, H)**, and 9 days **(I, J)** after 1.0 mm depth CCI. Injury with a flat-tip impactor **(A, C, E)**, created more profound tissue disruption, hemorrhage and cell loss within the first 12 h when compared to injury with a rounded tip impactor **(B, D, F)**. By 24 h and 9 days post-injury, tissue damage resulting from the flat-tip **(G, I)** and rounded-tip **(H, J)** impactor was similar. Arrows mark the approximate location of the edges of the craniotomy. Arrowheads note the location of tissue hemorrhage and neuron loss, corresponding to the path of the impactor edges, at 1 h after impact.

Quantification of cortical tissue damage

To quantify cortical damage, the boundaries of the neocortex containing morphologically identifiable neurons were outlined ipsilateral and contralateral to the impact on Nissl-stained coronal sections. Gross patterns of early neocortical distortion and cell death are shown in representative tracings in Figure 6A. Within the swollen ipsilateral cortex, two regions of neocortical damage are clearly evident at 1 h after CCI with a flat-tip impactor, consistent with the regions of acute hemorrhage and neuron loss illustrated in Figure 4A, and corresponding closely to the regions of high principle strains predicted by finite element model simulation (Fig. 2B, left panels). At 1 h after CCI with a rounded-tip impactor, neocortical tissue exhibited swelling at the craniotomy site, but overt tissue damage was only noted at 4 h. The volume of neocortical tissue damage increased significantly over time [main effect of time, $F(4, 38) = 52.15$, $p < 0.00001$; Fig. 6B]. The temporal progression was strongly dependent upon the tip geometry used to create the injury [interaction of tip and time, $F(4, 38) = 11.70$, $p < 0.00001$]. At 1 h post-injury, both groups exhibited negative contusion volumes caused by neocortical swelling and herniation (see also Fig. 4A,B and 6A). By 4 h post-injury, the amount of cortical damage increased significantly for the group injured with the flat tip ($p < 0.0005$ compared to 1 h) but not for the group injured with the rounded-tip impactor. No further increase in contusion volume was measured for mice injured using the flat-tip impactor, suggesting that the majority of neocortical damage occurred by 4 h post-injury. In contrast, mice injured with a rounded-tip impactor showed a progressive increase in contusion volume from 4 h to 12 h ($p < 0.001$) and from 12 h to 24 h ($p < 0.001$). Cortical tissue damage was greater with the flat-tip impactor than the rounded-tip impactor at both 4 h ($p < 0.0005$) and 12 h ($p < 0.005$), but was equivalent at 24 h and 9 days. These data demonstrate that CCI injury with a

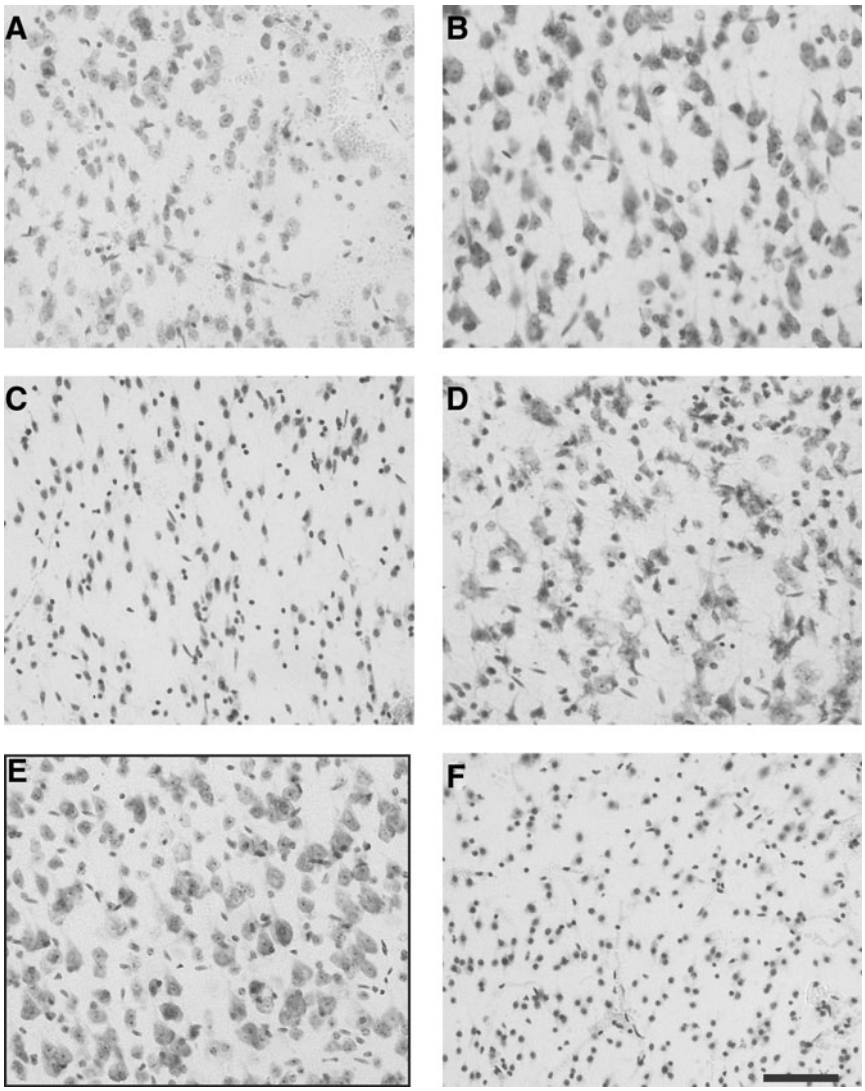

FIG. 5. Alterations in neocortical neuron morphology as a function of impactor tip shape. Compared to sham injury (**E**, with black border), cortical injury with a flat-tip impactor **(A)** results in more severe neuron shrinkage and loss of neuronal Nissl staining at 1 h than injury with a rounded-tip impactor **(B)**. Neuron death is more rapid with the flat-tip impactor, with nearly complete loss of cells with identifiable neuronal morphology by 4 h **(C)**, whereas morphological damage increases progressively from 4 h **(D)** to 12 h **(F)** after injury with a rounded-tip impactor. Scale bar represents 100 μm.

rounded-tip impactor resulted in a slower evolution of neocortical cell death over the first 12 h, but ultimately the same volume of cortical tissue damage, as compared to injury with a flat-tip impactor.

Regional hippocampal neurodegeneration

Fluorojade staining was used to evaluate acute regional neurodegeneration in the hippocampus. Only a few faintly labeled neurons were observed at 1 h post-injury (data not shown). At 4, 12, and 24 h, Fluorojade-positive neurons were clearly visible in both groups of mice after 1.0-mm CCI brain injury. Injury with a flat-tip impactor produced widespread neurodegeneration in the granule layers and hilus of the dentate gyrus and in the CA3 pyramidal layer, with less degeneration in the CA1 pyramidal layer (Fig. 7A, C, E). Neurodegeneration was most prevalent in the dentate gyrus following injury with a rounded-tip impactor, with fewer Fluorojade-positive neurons in the CA3 pyramidal layer and very few, if any, in the CA1 region (Fig. 7B, D, F).

Fluorojade-positive neurons were counted in the ipsilateral hippocampus at 4, 12, and 24 h post-injury. In the dentate gyrus, there was no overall effect of tip geometry or time, but the interaction between these variables was significant [$F(2,24) = 6.15$, $p < 0.01$; Fig. 8]. The flat-tip impactor caused an initial wave of neurodegeneration in the dentate gyrus at 4 h that was reduced by 12 h, although this decrease did not reach statistical significance ($p = 0.06$). The number of Fluorojade-positive dentate gyrus neurons increased from 12 h to 24 h after injury with the flat-tip impactor ($p < 0.05$). Numbers of degenerating dentate gyrus neurons did not change over time for the group injured with a rounded-tip impactor, and the numbers were not different from those of the flat-tip impactor group at any individual time point. In the CA3/CA3c pyramidal layer, CCI with the flat-tip impactor resulted in significantly greater neurodegeneration across the first 24 h when compared to CCI with the rounded-tip impactor [main effect of tip shape, $F(1,24) = 7.30$, $p < 0.05$; Fig. 8]. Numbers of Fluorojade-positive cells decreased from 4 h to 12 h ($p < 0.05$) and then increased again at 24 h ($p < 0.05$ compared to 12 h), a temporal trend that appeared more pronounced for the flat-tip impactor. Injury with a flat-tip impactor also produced greater neuron death in the CA1 region than did injury with the rounded-tip impactor [main effect of tip shape, $F(1,24) = 22.90$, $p < 0.0001$; Fig. 8], an effect that was time dependent [interaction of tip and time, $F(2, 24) = 4.10$, $p < 0.05$]. At 4 h, numbers of Fluorojade-labeled CA1 neurons were more than tenfold higher after injury with a flat-tip impactor than with a rounded-tip impactor ($p < 0.001$), and were significantly higher than those at 12 h or 24 h for either tip geometry ($p < 0.05$), indicating a very acute wave of CA1 cell death induced only by the flat-tip impactor.

BBB damage

Regional patterns of BBB breakdown were comparable after CCI injury using a flat-tip or rounded-tip impactor. At 1 h, IgG extravasation was localized to the impact site spanning neocortical layers I through VI, as well as the subcortical white matter and CA1 stratum oriens (Fig. 9A, B). By 4 h, BBB disruption had extended beyond the impact site in the neocortex and encompassed the entire ipsilateral hippocampus at the level of the impact epicenter (Fig. 9C, D). At 12 and 24 h, in

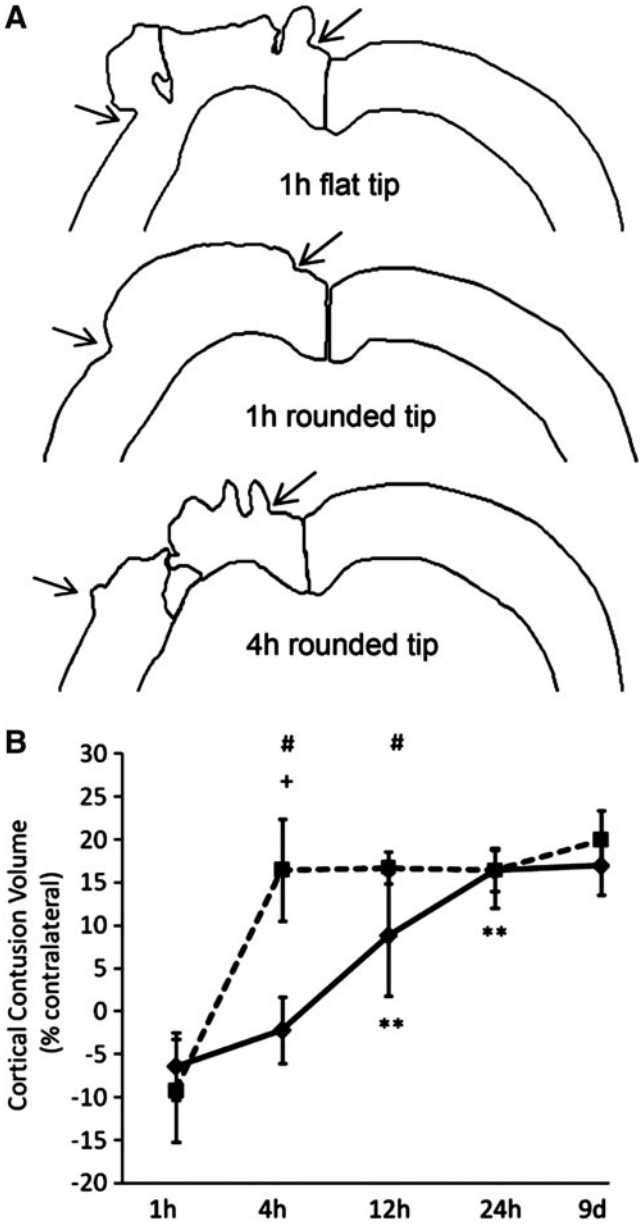

FIG. 6. Quantification of cortical tissue damage. **(A)** Representative tracings of the dorsal regions of the ipsilateral and contralateral neocortex containing morphologically identifiable neurons at the epicenter of injury 1h after impact with a flat-tip impactor and 1 h and 4 h after injury with a rounded-tip impactor. Arrows mark the location of the craniotomy edges as in Figure 4. **(B)** The volume of cortical damage produced by injury with a flat-tip impactor was maximal by 4 h and was unchanged out to 9 days. In contrast, cortical injury with a rounded-tip impactor led to a more slowly developing cortical contusion that increased in size over 24 h, reaching a contusion volume equivalent to that of the flat-tip impactor group. Square symbols denote flat-tip impactor group means; diamond symbols denote round-tip impactor group means. Error bars represent standard deviations. ($+p < 0.0005$ compared to the previous time point for the flat-tip impactor group; $^{**}p < 0.001$ compared to the previous time point for the rounded-tip impactor group; # $p < 0.005$ comparing flat-tip and rounded-tip impactor groups at the same time point).

addition to the robust IgG immunostaining in the ipsilateral cortex, subcortical white matter and hippocampus, faint IgG labeling was observed in the dorsal thalamus and in the contralateral cortex and hippocampus near midline. At 9 days, IgG extravasation was less pronounced than at 24 h.

Traumatic axonal injury

Traumatic axonal injury was assessed qualitatively using immunohistochemistry for APP, a well-established marker of axonal injury. Impact to the cortex with either a flat-tip or rounded-tip impactor resulted in acute axonal injury throughout cortical and subcortical structures in the ipsilateral hemisphere. There were no overt differences in the distribution or time course of axonal injury between the two tip geometries. From 1 h to 24 h post-injury, axonal injury was evident along the edges of the impact site in the neocortex, and in the deep neocortex (layer VI) and the subcortical white matter tract below the impacted cortex (Fig. 10A, B). APP-positive injured axons were also observed in the dorsal

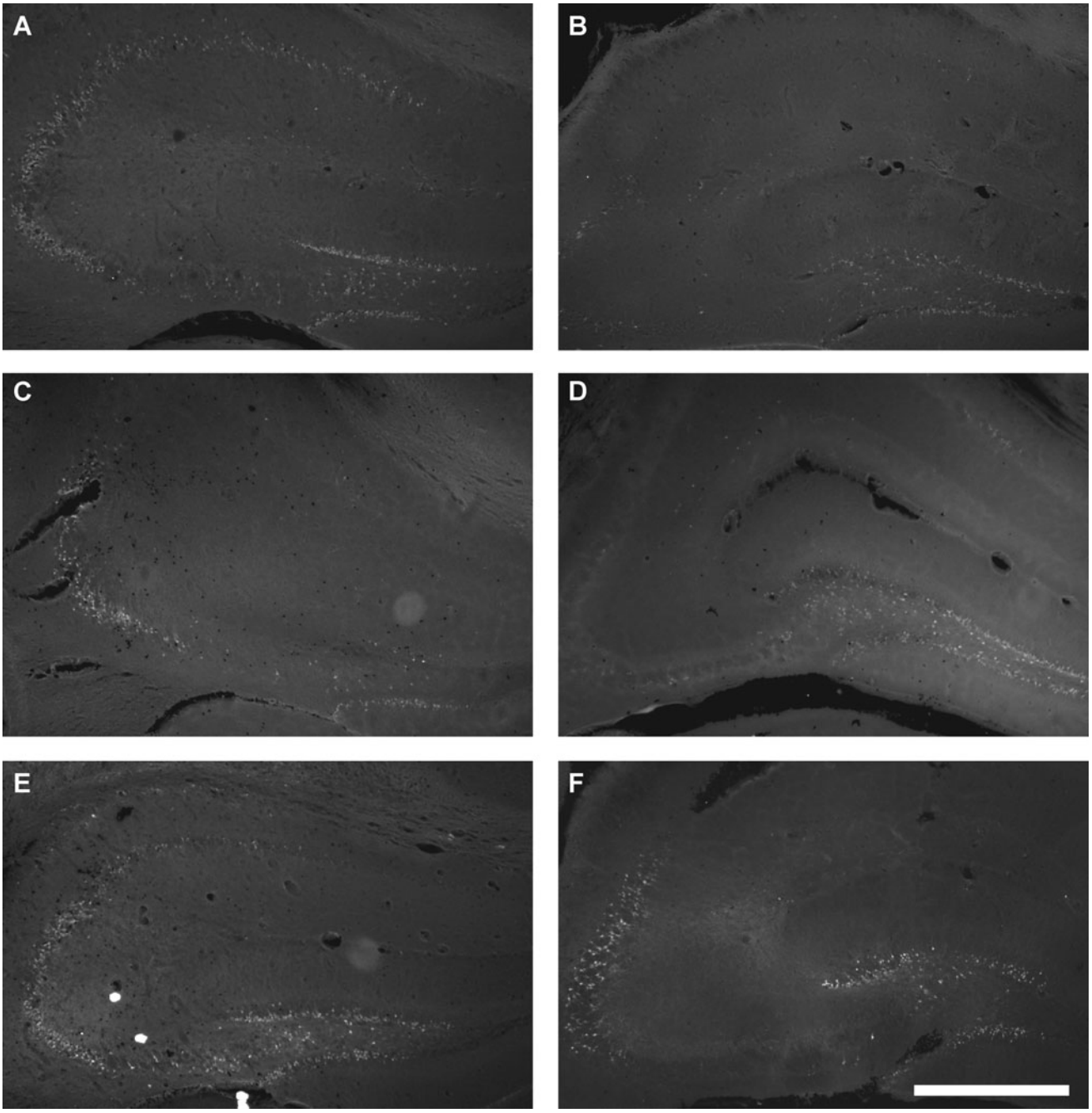

FIG. 7. Hippocampal neurodegeneration after CCI with a flat-tip **(A, C, E)** or a rounded- tip **(B, D, F)** impactor. Fluorojade-B staining of sections taken at the impact epicenter illustrate degenerating neurons in the dentate gyrus granule layers, dentate hilus, and CA3 and CA1 pyramidal layers at 4 h **(A, B)**, 12 h **(C, D),** and 24 h **(E, F)** after 1.0-mm CCI brain injury. Scale bar represents 500 μm.

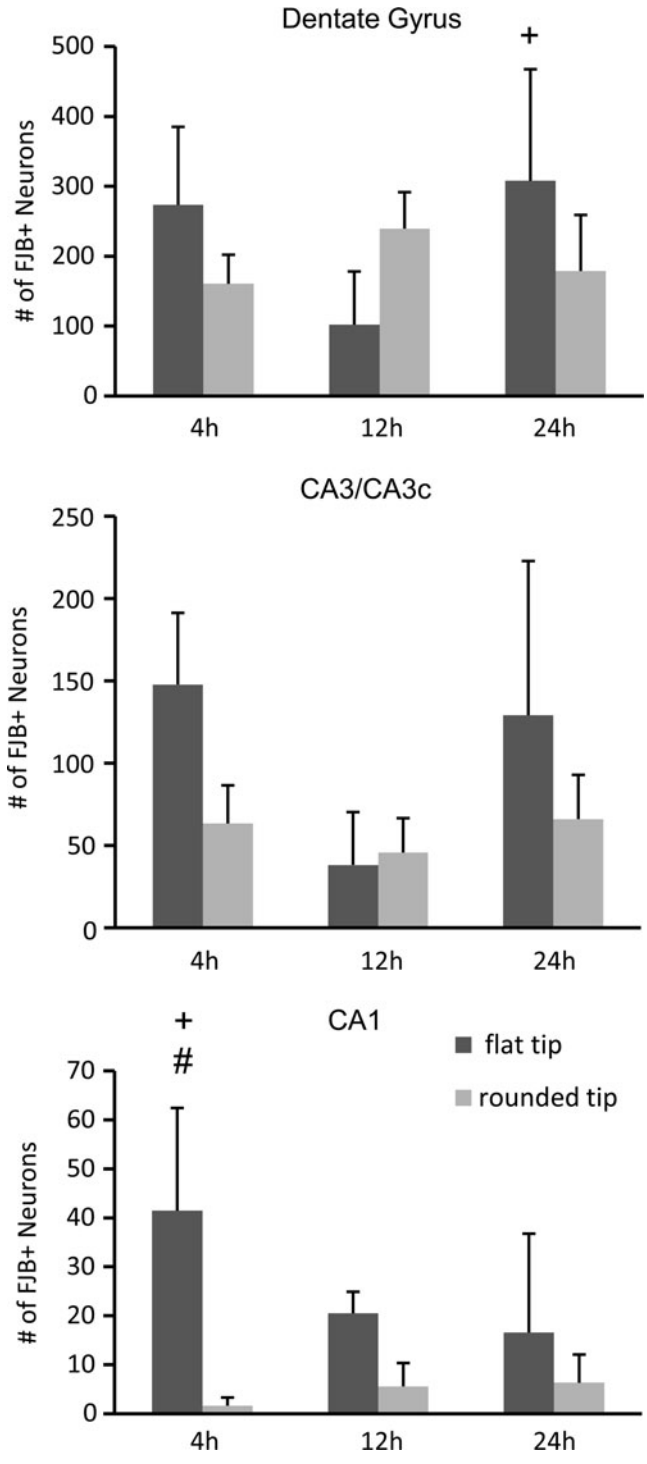

FIG. 8. Quantification of regional hippocampal neurodegeneration as a function of impactor tip shape. Fluorojade-B positive (FJB+) neurons were counted in the dentate gyrus, including the granule layers and hilar region, CA3/CA3c pyramidal layer, and CA1 pyramidal layer at 4 h, 12 h, and 24 h after brain injury with a flat-tip impactor (dark grey bars) or rounded-tip impactor (light gray bars). Data are shown as means + standard deviation. ($+p < 0.05$ compared to the adjacent time point for the flat tip impactor group; $\#p < 0.001$ comparing flat tip and rounded tip impactor groups at the same time point).

ipsilateral thalamus (Fig. 10C, D) and occasionally within the hippocampus, most often in the stratum oriens of the CA3 and CA1 regions and along the hippocampal fissure. Qualitatively, the frequency and staining intensity of APP-positive axons increased from 1 h to 12 h. No axonal injury was observed in the contralateral hemisphere for any of the time points for either tip shape.

Motor and cognitive behavioral outcome

Deficits in coordinated motor function were evaluated using a modified NSS at 1 h and 1, 2, 5, and 7 days after CCI brain injury. Tip geometry was not a factor in determining the level of initial motor dysfunction or the rate of recovery of function (Fig. 11A). Both groups of brain-injured mice exhibited profound motor deficits using the NSS at 1 h post-injury and a significant spontaneous recovery over time [main effect of time, $F(4,32) = 37.71$, $p < 0.0001$]. Similarly, evaluation of basic motor functions including limb flexion, extension, and grip strength using a composite neuroscore revealed equivalent deficits in mice injured using either a flat-tip or rounded-tip impactor (Fig. 11B). Both groups of mice showed notable motor dysfunction at 1 day after CCI, and significant recovery of function over time [main effect of time, $F(3,24) = 14.26$, $p < 0.0001$].

As with post-traumatic motor deficits, the use of a flat-tip or rounded-tip impactor did not significantly alter post-traumatic cognitive function assessed in an MWM at 1 week after severe CCI (Fig. 11C). Learning latencies were equivalent for the two groups, with both achieving significantly lower latencies to the platform on days 8 and 9 compared to day 7 ($p < 0.0005$).

Discussion

The CCI model of contusion brain injury is one of the most widely used models of TBI in mice. Mouse models are being increasingly used to exploit transgenic and knockout technologies for the study of specific proteins or for expression of tissue- or cell-specific reporters. The low cost and small body weight of mice are also attractive for testing therapeutic interventions, especially when large cohorts are needed to perform comprehensive dose response studies or test behavioral outcomes. We have demonstrated that in the mouse CCI model the rate of neocortical neurodegeneration is highly dependent upon the shape of the impactor tip. A 1.0-mm depth injury with a flat-tip impactor results in significantly faster cortical neuron death, more pronounced acute hemorrhage, and greater initial hippocampal neurodegeneration than injury with a rounded-tip impactor. Injury severity, assessed by (1) impact depth and velocity, (2) the size of the neocortical contusion at 9 days after injury, (3) the presence or pattern of BBB breakdown and axonal injury, and (4) the magnitude of neurobehavioral deficits, was equivalent for the two impactors. These data suggest that rounding the tip of the impactor slows the temporal course of the neurovascular damage without reducing or eliminating important pathophysiological features of CCI brain injury.

A three-dimensional finite element model was used to predict tissue strains in response to a 1.0-mm 3.5-m/s CCI injury using a flat-tip or rounded-tip impactor. Maximum principal strains were predicted to be substantially higher for the flat-tip impactor than for the rounded-tip impactor. For

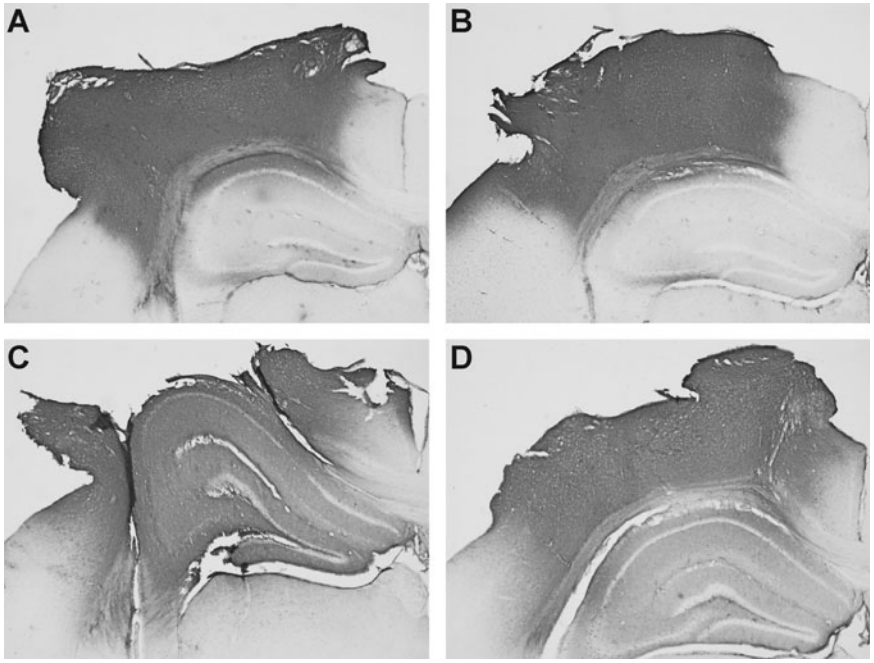

FIG. 9. Acute BBB damage after severe controlled cortical impact using a flat-tip impactor **(A, C)** or a rounded tip impactor **(B, D)**. The location and progression of extravasation of IgG was similar for injury with the flat-tip and rounded-tip impactors, as illustrated at 1 h **(A**, **B)** and 4 h **(C, D)** after injury.

the flat-tip impactor, tissue strains were predicted to be highest around the edge of the impactor as it penetrated the cortical parenchyma. Histological damage, including hemorrhage and loss of Nissl stain, was indeed observed most frequently at the boundaries of the impactor's path as early as 1 h after injury with a flat-tip impactor (see Figs. 4 and 6). Interestingly, the strain at which human cerebral arteries fail under dynamic elongation *ex vivo* is estimated to be 0.50, or 50% (Monson et al., 2003). Based on these data, arterial rupture or tearing would be predicted along the edges of the path of the flat-tip impactor, consistent with the presence of hemorrhage in this region. For the rounded-tip impactor, maximum strains were predicted to be centered beneath the impactor, more diffusely distributed in the deep cortex, consistent with strain contours generated for CCI injury in the rat (Mao et al., 2010b). One limitation of the current mouse brain model is that the finite element meshes were morphed from the previously validated rat brain model with some adjustments made on the brain outer surface, ventricles, and white matter. Gray matter structures were assigned the same material properties. Detailed meshes representing other anatomical parts, such as hippocampus or thalamus, and incorporation of region-specific material property heterogeneities, are required in the future to improve the biofidelity of this model. Testing mouse brains to acquire mouse-specific properties would increase the prediction accuracy of the numerical mouse brain model. Tears within the brain parenchyma during impact would necessarily alter the strain pattern in neighboring regions. However, micro-tearing of brain tissues or intracranial vasculatures was not addressed in our finite element model because a much higher resolution brain model would be needed for predicting such injuries. Unfortunately, a very fine mesh model is computationally challenging at present. Even if such a model existed and were computationally feasible, very little is known about strain thresholds for individual cellular components within the brain.

Dynamic strains of ≥ 0.10–0.20 (10–20%) are sufficient to elicit morphological signs of injury or dysfunction in neurons or axons (Bain and Meaney, 2000; Cater et al., 2006; Elkin and Morrison, 2007; Geddes et al., 2003a). During focal or diffuse TBI, tissue deformation leads to early compromise of the normal selective barrier function of the plasmalemma (Farkas et al., 2006; Whalen et al., 2008), contributing to ion dysregulation (Kilinc et al., 2009). Both enhanced neuronal membrane permeability and increases in intracellular free calcium have been shown to be proportional to applied strain (Geddes et al., 2003a; LaPlaca et al., 1997), suggesting that in regions of highest tissue strains, neurons will more likely experience greater and more sustained calcium perturbations, which could lead to mitochondrial dysfunction, protease activation and cell death. While trauma-induced membrane permeability increases may be transient under some conditions, sustained leakiness results in cell death (Farkas et al., 2006; Geddes et al., 2003a,b; LaPlaca et al., 1997). Collectively, these studies are consistent with the premise that higher strains generated by a flat-tip impactor would be associated with more severe membrane permeability alterations and calcium dysregulation with less likelihood of recovery, resulting in rapid cell death. Recent work supports a direct correlation between maximum principal strains predicted by finite element modeling and the degree of neuronal degeneration in a rat model of CCI brain injury (Mao et al., 2010a).

Quantification of the progression of cell death within the ipsilateral neocortex following severe contusion injury with either a flat- or rounded-tip impactor revealed marked differences in the evolution of neocortical damage. Injury with a flat-tip impactor produced rapid cell death, with maturation of the neocortical lesion by 4 h, whereas impact

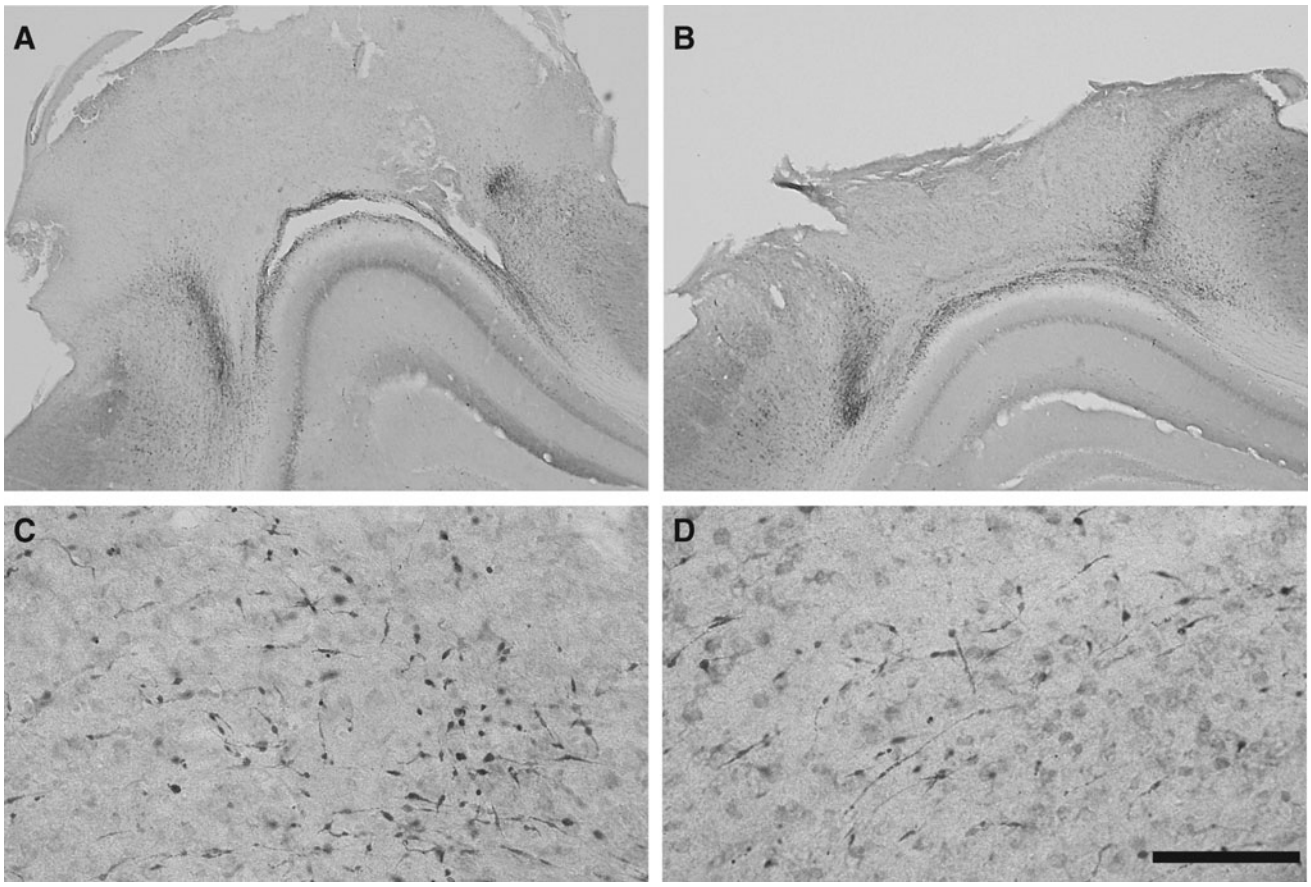

FIG. 10. Traumatic axonal injury induced by injury with either a flat-tip **(A, C)** or rounded-tip **(B, D)** impactor. The spatial patterns of axonal injury, detected using immunohistochemistry for amyloid precursor protein, were similar for mice injured with a flat- tip or rounded-tip impactor. In the neocortex, axonal injury was concentrated around the periphery of impact site and in the subjacent white matter and gray matter/white matter interface (12 h postinjury shown; **A, B**). Axonal injury was also clearly evident in subcortical structures such as the hippocampus (not shown) and dorsal thalamus (24 h shown; **C, D**; scale bar represents 200 μm).

with a rounded tip resulted in milder initial neocortical damage that progressively increased out to 24 h post-injury to a level equivalent to that produced by the flat-tip impactor. Although relatively little information is available on the acute time course of cortical damage after CCI, our findings are consistent with previous studies using CCI with a flat-tip impactor in mice. Using propidium iodide exclusion as an indicator of membrane integrity, Whalen and associates (2008) reported marked increases in plasma membrane compromise in the cortex at 1 h after 0.6-mm, 6-m/s CCI, after which most membrane-compromised neurons degenerated. Similarly, Hall and colleagues (Hall et al., 2008; Thompson et al., 2006) demonstrated that the size of the cortical cavitation (lesion volume) is fully developed by 6 h after 1.0-mm, 3.5-m/s CCI. In the CCI model, the amount of neocortical cell death can be altered by changing the depth or velocity of impact in the mouse (Fox et al., 1998; Hannay et al., 1999; Saatman et al., 2006) and rat (Goodman et al., 1994; Sutton et al., 1993). However, because these histological evaluations were typically performed days to weeks after the injury, it is unclear to what extent velocity or depth of impact affects the rate of cortical neurodegeneration. Injury severity and the rate of cell death may also vary for different injury devices. Fox et al. (1998) use a custom-made CCI device with a flat-tip impactor and reported no cortical cavitation at 7 days after a 1-mm depth, 4.5-m/s injury to C57BL/6 mice. Nevertheless, a 1-mm impact at a higher velocity (6 m/s) resulted in neocortical neurodegeneration concentrated at the periphery of the flat-tip impactor, a pattern consistent with our finite element predictions, as described previously.

In addition to a prominent neocortical contusion, CCI brain injury typically results in neuron loss in the hippocampal dentate gyrus and CA3 pyramidal layers (Baldwin et al., 1997; Goodman et al., 1994; Hall et al., 2008; Saatman et al., 2006; Smith et al., 1995). Although the CA3 sub-region is positioned further from the impact than the CA1 region, CA3 neurons appear more vulnerable to CCI, perhaps because of greater tissue compliance within the CA3 region compared to the CA1 region (Elkin et al., 2010). However, involvement of the CA1 pyramidal layer is also often reported as impact depth is increased (Goodman et al., 1994; Saatman et al., 2006; Scheff et al., 1997; Whalen et al., 2008). Quantification of degenerating neurons revealed that the rates and extent of neurodegeneration within the hippocampus are altered by the impactor tip geometry. Injury with a flat-tip impactor produced a wave of acute neurodegeneration at 4 h, with the largest number of degenerating cells in the dentate gyrus, followed by the CA3 and then the CA1 regions. A similar

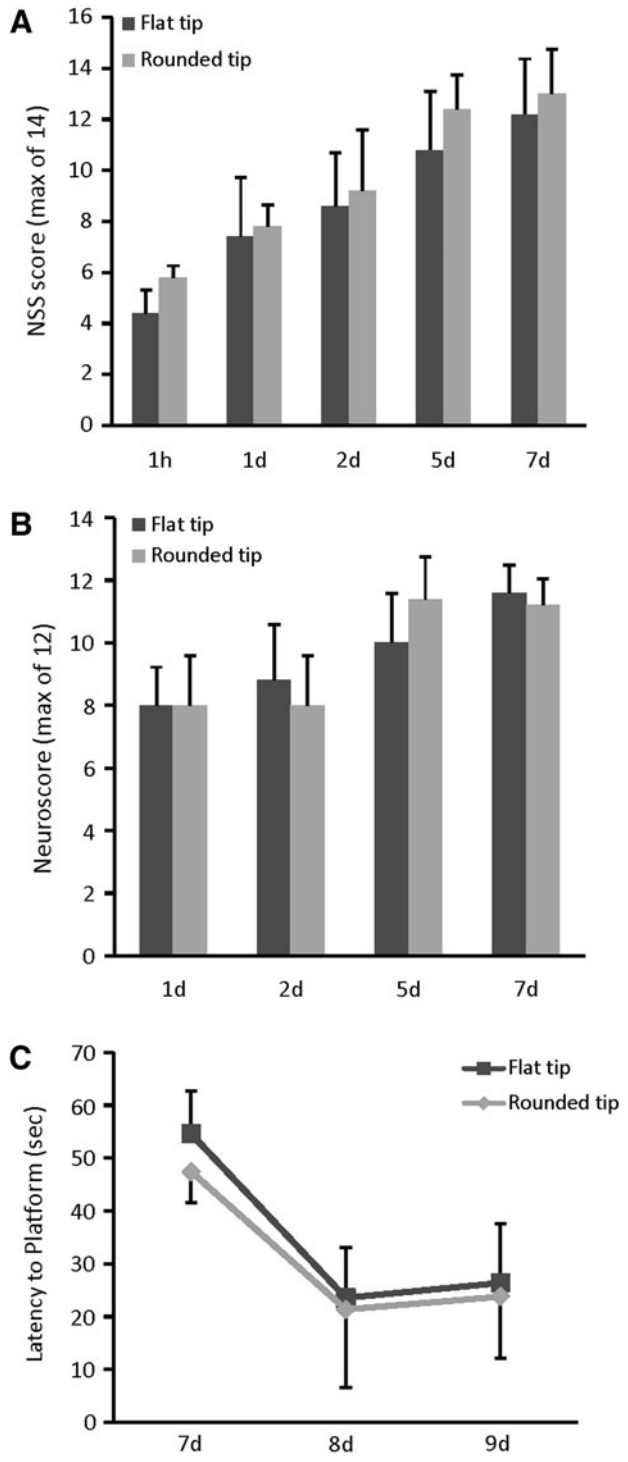

FIG. 11. Effect of impactor tip shape on neurological motor and cognitive function of mice subjected to cortical impact injury. Mice injured with a flat-tip impactor or a rounded-tip impactor exhibited equivalent motor deficits over the first week after injury, when measured using **(A)** a 14-point modified neurological severity score (NSS) or **(B)** a 12-point composite neuroscore. **(C)** Impactor tip shape also had no significant effect on the ability to learn the location of a hidden platform in a MWM over a 3-day testing period. Dark gray bars or square symbols denote flat-tip impactor group means; light grey bars or diamond symbols denote round-tip impactor group means. Error bars represent standard deviations.

acute phase (peak at 1–6 h) and regional distribution of degenerating neurons with plasma membrane compromise was reported for mouse CCI with a flat-tip impactor (Whalen et al., 2008). In contrast, impact with a rounded tip appeared to produce a more consistent progression of hippocampal neurodegeneration across the first 24 h after injury, with minimal involvement of the CA1 region. Early hippocampal neurodegeneration may be more extensive following injury with the flat-tip impactor as a result of larger tissue displacement during impact, with the bulk of the cortical tissue being forced downward into the hippocampal structure. Despite the slightly larger diameter of the rounded tip, a much smaller volume of tissue is displaced and some of the cortical tissue may be compressed and deformed laterally, reducing the deformation of the hippocampus. Results predicted by the finite element model corroborate this assumption. A peak maximum principal strain of 30.1% was induced using the flat impactor whereas the corresponding value was 24.8% for the rounded impactor. Despite the lower strains that occur in the hippocampus compared to the neocortex with CCI, hippocampal neurons *in vitro* exhibit larger intracellular calcium increases and more cell death compared to cortical neurons in response to stretch injury, suggesting an enhanced vulnerability to traumatic stimuli (Elkin and Morrison, 2007; Geddes et al., 2003b).

BBB breakdown is an important aspect of cerebrovascular damage in TBI (DeWitt and Prough, 2003) that has been reproduced in severe CCI (Hicks et al., 1997; Smith et al., 1995). In this study, damage to the BBB was visualized by IgG immunoreactivity within the ipsilateral neocortex and hippocampus in patterns similar for both impactor tips. Extravasation of IgG was localized primarily to the neocortex at 1 h, whereas at 4 h post-injury IgG labeling was also observed in the hippocampus, as previously reported (Saatman et al., 2006). Regional patterns of disruption of the BBB in mice were not substantially modulated in the present study by impactor tip geometry, or by severity of injury (impact depth) for CCI injury with a rounded-tip impactor (Saatman et al., 2006), suggesting that the threshold for mechanically stimulated BBB damage may be low, and that compromise of the BBB may be a common pathology across a range of injury severities. Our analysis of BBB breakdown is limited in that it was not quantitative, leaving open the possibility that the degree of extravasation caused by the two tips may be different. In addition, IgG extravasation yields limited information about the time course of BBB disruption. Further studies with Evan's Blue administered intravascularly at various post-injury time intervals could provide more information regarding the time course of BBB disruption or recovery for these two injury paradigms. Nonetheless, our data confirm that impact injury with a rounded tip results in neocortical and hippocampal BBB damage, reproducing an important aspect of CCI pathology associated with secondary injury cascades such as inflammation and oxidative stress.

Axons are vulnerable to stretch injury induced by tensile/shear strains within the brain tissue. Traumatic axonal injury results in rapidly altered membrane permeability, intracellular calcium imbalances and mitochondrial damage, protease activation, and disruption in axonal transport (Saatman et al., 2009). Injured axons are a vital therapeutic target in diffuse brain injury, representing the defining pathology in diffuse axonal injury. Sparing axonal integrity may also be important

in focal brain trauma. Even in models designed to produce focal contusions, such as the CCI model, axonal damage is present in several regions outside the contused neocortex, such as the hippocampus and thalamus (Dunn-Meynell and Levin, 1997; Hall et al., 2005, 2008; Lighthall et al., 1990). Here we show that impact with either a rounded- tip or flat-tip impactor produced axonal injury within the contused neocortex and the underlying hippocampus and thalamus. Although the number of injured axons was not quantified, the onset and overall distribution of axonal injury was comparable for the two tip geometries.

In pre-clinical evaluation of therapeutic approaches for TBI, behavioral deficits are an especially important outcome measure. Both motor and cognitive deficits have been well described in both rat and mouse models of TBI, utilizing a number of different behavioral tasks (Fujimoto et al., 2004; Hamm, 2001). The severity of behavioral dysfunction can be altered by changing certain biomechanical aspects of CCI injury, such as the depth (Saatman et al., 2006; Yu et al., 2009) or velocity (Fox et al., 1998) of impact. Despite the fact that CCI brain injury with a flat-tip impactor resulted in greater maximal tissue strains than impact with a rounded tip, motor and cognitive functions of brain-injured mice were not grossly influenced by impactor tip geometry, although the small group sizes may have limited our ability to detect small differences. Behavior was evaluated at several times after injury using a composite neuroscore, neurological severity score, and a MWM learning task. This suggests that slowing the progression of cortical cell death through the use of a rounded tip did not compromise the fidelity of the behavioral response. Brain injury-induced neuromotor or cognitive impairments in CCI-injured mice have been attenuated through various treatment approaches, illustrating the influence of secondary injury cascades on post-traumatic behavioral responses (Clausen et al., 2009; Longhi et al., 2009; Mbye et al., 2009; You et al., 2008). Therefore, the use of a rounded- tip impactor may provide a greater therapeutic window for targeting acute cell dysfunction or death without diminishing the power of the CCI model for the evaluation of behavioral impairment and recovery.

In summary, we have quantitatively and qualitatively investigated the effects of impactor tip geometry on predicted tissue strains, histological outcomes, and behavioral responses following severe lateral CCI brain injury in mice. Compared to CCI with the commonly used flat-tip impactor, injury with a rounded-tip impactor resulted in more uniform maximum principal strains with lower peak magnitudes, reduced acute neurovascular disruption, and a slower progression of neocortical cell death. A more gradual evolution of neocortical neuronal death was achieved with a rounded-tip CCI without altering the size of neocortical contusion at 9 days after injury or substantially changing other clinically relevant aspects of this brain injury model such as BBB breakdown, axonal injury, or neurobehavioral dysfunction. By slowing the progression of neuronal damage, the CCI model may better mimic the evolution of contusive damage in human TBI. Furthermore, lengthening the time between the primary insult and the eventual death of the cell is advantageous for mechanistic studies aimed at distinguishing the onset, duration, and interactions of upstream and downstream events, or isolating specific aspects of injury cascades. Slowing the time course of neuronal death also yields a longer therapeutic window, increasing the likelihood that therapeutic compounds can be administered using a clinically relevant post-injury paradigm, reach therapeutic levels in the central nervous system, and affect the desired targets. These data suggest that along with impact depth and velocity, impactor tip shape is an important determinant of acute tissue response to rapid impact brain injury. Therefore, in studies of acute injury mechanisms of contusive TBI or in evaluations of therapeutic interventions targeting neuronal death, impactor tip geometry should be carefully considered.

Acknowledgments

This work was funded by NIH P01 NS058484, P30 NS051220 and KSCHIRT 6-12 and 7-20 (K.E.S.), KSCHIRT 8-15A (S.W.S.), and by the Injury Control Research Center at University of Alabama at Birmingham (K.Y.).

Author Disclosure Statement

No competing financial interests exist.

References

Alahmadi, H., Vachhrajani, S., and Cusimano, M.D. (2010). The natural history of brain contusion: an analysis of radiological and clinical progression. J. Neurosurg. 112,1139–1145.

Anderson, K.J., Miller, K.M., Fugaccia, I., and Scheff, S.W. (2005). Regional distribution of fluoro-jade B staining in the hippocampus following traumatic brain injury. Exp. Neurol. 193,125–130.

Bain, A.C., and Meaney, D.F. (2000). Tissue-level thresholds for axonal damage in an experimental model of central nervous system white matter injury. J. Biomech. Eng. 122, 615–622.

Baldwin, S.A., Gibson, T., Callihan, C.T., Sullivan, P.G., Palmer, E., and Scheff, S.W. (1997). Neuronal cell loss in the CA3 subfield of the hippocampus following cortical contusion utilizing the optical disector method for cell counting. J. Neurotrauma 14,385–398.

Cater, H.L., Sundstrom, L,E,, and Morrison, B., 3rd. (2006). Temporal development of hippocampal cell death is dependent on tissue strain but not strain rate. J. Biomech. 39, 2810–2818.

Clausen, F., Hanell, A., Bjork, M., Hillered, L., Mir, A.K., Gram, H., and Marklund, N. (2009). Neutralization of interleukin-1beta modifies the inflammatory response and improves histological and cognitive outcome following traumatic brain injury in mice. Eur. J. Neurosci. 30, 385–396.

Dennis, A.M., Haselkorn, M.L., Vagni, V.A., Garman, R.H., Janesko-Feldman, K., Bayir, H., Clark, R,S., Jenkins, L.W., Dixon, C.E., and Kochanek, P.M. (2009). Hemorrhagic shock after experimental traumatic brain injury in mice: effect on neuronal death. J Neurotrauma 26,889–899.

DeWitt, D.S., and Prough, D.S. (2003). Traumatic cerebral vascular injury: the effects of concussive brain injury on the cerebral vasculature. J Neurotrauma 20,795–825.

Dixon, C.E., Clifton, G.L., Lighthall, J.W., Yaghmai, A.A., and Hayes, R.L. (1991). A controlled cortical impact model of traumatic brain injury in the rat. J. Neurosci. Methods 39, 253–262.

Dunn-Meynell, A.A., and Levin, B.E. (1997). Histological markers of neuronal, axonal and astrocytic changes after lateral rigid impact traumatic brain injury. Brain Res. 761, 25–41.

Elkin, B.S., Ilankovan, A., and Morrison, B., 3rd. (2010). Age-dependent regional mechanical properties of the rat hippocampus and cortex. J. Biomech. Eng. 132: 011010.

Elkin, B.S., and Morrison, B., 3rd. (2007). Region-specific tolerance criteria for the living brain. Stapp Car Crash J. 51,127–138.

Farkas, O., Lifshitz, J., and Povlishock, J.T. (2006). Mechanoporation induced by diffuse traumatic brain injury: an irreversible or reversible response to injury? J.Neurosci. 26, 3130–3140.

Fox, G.B., Fan, L., LeVasseur, R.A., and Faden, A.I. (1998). Sustained sensory/motor and cognitive deficits with neuronal apoptosis following controlled cortical impact brain injury in the mouse. J.Neurotrauma. 15, 599–614.

Fujimoto, S.T., Longhi, L., Saatman, K.E., Conte, V., Stocchetti, N., and McIntosh, T.K. (2004). Motor and cognitive function evaluation following experimental traumatic brain injury. Neurosci. Biobehav. Rev. 28,365–378.

Galford, J.E., and McElhaney, J.H. (1970). A viscoelastic study of scalp, brain, and dura. J. Biomech. 3, 211–221.

Geddes, D.M., Cargill, R.S., 2nd, and LaPlaca, M.C. (2003a). Mechanical stretch to neurons results in a strain rate and magnitude-dependent increase in plasma membrane permeability. J. Neurotrauma 20,1039–1049.

Geddes, D.M., LaPlaca, M.C., and Cargill, R.S., 2nd. (2003b). Susceptibility of hippocampal neurons to mechanically induced injury. Exp. Neurol. 184,420–427.

Gefen, A., Gefen, N., Zhu, Q., Raghupathi, R., and Margulies, S.S. (2003). Age-dependent changes in material properties of the brain and braincase of the rat. J. Neurotrauma 20,1163–1177.

Goodman, J.C., Cherian, L., Bryan, R.M., Jr., and Robertson, C.S. (1994). Lateral cortical impact injury in rats: pathologic effects of varying cortical compression and impact velocity. J. Neurotrauma 11,587–597.

Hall, E.D., Bryant, Y.D., Cho, W., and Sullivan, P.G. (2008). Evolution of post-traumatic neurodegeneration after controlled cortical impact traumatic brain injury in mice and rats as assessed by the de Olmos silver and fluorojade staining methods. J Neurotrauma 25,235–247.

Hall, E.D., Sullivan, P.G., Gibson, T.R., Pavel, K.M., Thompson, B.M., and Scheff, S.W. (2005). Spatial and temporal characteristics of neurodegeneration after controlled cortical impact in mice: more than a focal brain injury. J. Neurotrauma 22, 252–265.

Hamm, R.J. (2001). Neurobehavioral assessment of outcome following traumatic brain injury in rats: an evaluation of seleced measures. J. Neurotrauma 18,1207–1216.

Hamm, R.J., Dixon, C.E., Gbadebo, D.M., Singha, A.K., Jenkins, L.W., Lyeth, B.G., and Hayes, R.L. (1992). Cognitive deficits following traumatic brain injury produced by controlled cortical impact. J. Neurotrauma 9, 11–20.

Hannay, H.J., Feldman, Z., Phan, P., Keyani, A., Panwar, N., Goodman, J.C., and Robertson, C.S. (1999). Validation of a controlled cortical impact model of head injury in mice. J. Neurotrauma 16:1103–1114.

Hicks, R.R., Baldwin, S.A., and Scheff, S.W. (1997). Serum extravasation and cytoskeletal alterations following traumatic brain injury in rats. Comparison of lateral fluid percussion and cortical impact models. Mol. Chem. Neuropathol. 32,1–16.

Jin, X., Lee, J.B., Leung, L.Y., Zhang, L., Yang, K.H., and King, A.I. (2006). Biomechanical response of the bovine pia-arachnoid complex to tensile loading at varying strain-rates. Stapp Car Crash J. 50, 637–649.

Kilinc, D., Gallo, G., and Barbee, K.A. (2009). Mechanical membrane injury induces axonal beading through localized activation of calpain. Exp. Neurol. 219,553–561.

LaPlaca, M.C., Lee, V.M.Y., and Thibault, L.E. (1997). An in vitro model of traumatic neuronal injury: loading rate-dependent changes in acute cytosolic calcium and lactate dehydrogenase release. J Neurotrauma 14,355–368.

Lighthall, J.W. (1988). Controlled cortical impact: a new experimental brain injury model. J Neurotrauma 5,1–15.

Lighthall, J.W., Goshgarian, H.G., and Pinderski, C.R. (1990). Characterization of axonal injury produced by controlled cortical impact. J.Neurotrauma 7,65–76.

Longhi, L., Perego, C., Ortolano, F., Zanier, E.R., Bianchi, P., Stocchetti, N., McIntosh, T.K., and De Simoni, M.G. (2009). C1-inhibitor attenuates neurobehavioral deficits and reduces contusion volume after controlled cortical impact brain injury in mice. Crit. Care Med. 37,659–665.

Ma, Y., Hof, P.R., Grant, S.C., Blackband, S.J., Bennett, R., Slatest, L., McGuigan, M.D., and Benveniste, H. (2005). A three-dimensional digital atlas database of the adult C57BL/6J mouse brain by magnetic resonance microscopy. Neuroscience 135,1203–1215.

Maas, A.I., Hukkelhoven, C.W., Marshall, L.F., and Steyerberg, E.W. (2005). Prediction of outcome in traumatic brain injury with computed tomographic characteristics: a comparison between the computed tomographic classification and combinations of computed tomographic predictors. Neurosurgery 57,1173–1182.

Maas, A.I., Roozenbeek, B., and Manley, G.T. (2010). Clinical trials in traumatic brain injury: past experience and current developments. Neurotherapeutics 7,115–126.

Maas, A.I., Steyerberg, E.W., Murray, G.D., Bullock, R., Baethmann, A., Marshall, L.F., and Teasdale, G.M. (1999). Why have recent trials of neuroprotective agents in head injury failed to show convincing efficacy? A pragmatic analysis and theoretical considerations. Neurosurgery 44,1286–1298.

Mao, H., Jin, X., Zhang, L., Yang, K.H., Igarashi, T., Noble-Haeusslein, L.J., and King, A.I. (2010a). Finite element analysis of controlled cortical impact-induced cell loss. J Neurotrauma 27,877–888.

Mao, H., Yang, K.H., King, A.I., and Yang, K. (2010b). Computational neurotrauma-design, simulation, and analysis of controlled cortical impact model. Biomech. Model Mechanobiol. 9, 763–772.

Mao, H., Zhang, L., Yang, K.H., and King, A.I. (2006). Application of a finite element model of the brain to study traumatic brain injury mechanisms in the rat. Stapp Car Crash J. 50,583–600.

Marshall, L.F., Marshall, S.B., Klauber, M.R., Van Berkum, C.M., Eisenberg, H., Jane, J.A., Luerssen, T.G., Marmarou, A., and Foulkes, M.A. (1992). The diagnosis of head injury requires a classification based on computed axial tomography. J.Neurotrauma 9, Suppl. 1, S287–S292.

Mbye, L.H., Singh, I.N., Carrico, K.M., Saatman, K.E., and Hall, E.D. (2009). Comparative neuroprotective effects of cyclosporin A and NIM811, a nonimmunosuppressive cyclosporin A analog, following traumatic brain injury. J. Cereb. Blood Flow Metab. 29,87–97.

Meaney, D.F., Ross, D.T., Winkelstein, B.A., Brasko, J., Goldstein, D., Bilston, L.B., Thibault, L.E., and Gennarelli, T.A. (1994). Modification of the cortical impact model to produce axonal injury in the rat cerebral cortex. J. Neurotrauma 11,599–612.

Monson, K.L., Goldsmith, W., Barbaro, N.M., and Manley, G.T. (2003). Axial mechanical properties of fresh human cerebral blood vessels. J. Biomech. Eng. 125,288–294.

Narayan, R.K., Michel, M.E., Ansell, B., Baethmann, A., Biegon, A., Bracken, M.B., Bullock, M.R., Choi, S.C., Clifton, G.L., Contant, C.F., Coplin, W.M., Dietrich, W.D., Ghajar, J., Grady,

S.M., Grossman, R.G., Hall, E.D., Heetderks, W., Hovda, D.A., Jallo, J., Katz, R.L., Knoller, N., Kochanek, P.M., Maas, A.I., Majde, J., Marion, D.W., Marmarou. A., Marshall, L.F., McIntosh, T.K., Miller, E., Mohberg, N., Muizelaar, J.P., Pitts, L.H., Quinn, P., Riesenfeld, G., Robertson, C.S., Strauss, K.I., Teasdale, G., Temkin, N., Tuma, R., Wade, C., Walker, M.D., Weinrich, M., Whyte, J., Wilberger, J., Young, A.B., and Yurkewicz, L. (2002). Clinical trials in head injury. J.Neurotrauma 19,503–557.

Paxinos, G., and Franklin, K.B.J. (2001). *The Mouse Brain in Stereotaxic Coordinates*, 2nd ed. Academic Press: San Diego.

Prins, M.L., and Hovda, D.A. (2001). Mapping cerebral glucose metabolism during spatial learning: interactions of development and traumatic brain injury. J Neurotrauma 18,31–46.

Royo, N.C., Conte, V., Saatman, K.E., Shimizu, S., Belfield, C.M., Soltesz, K.M., Davis, J.E., Fujimoto, S.T., and McIntosh, T.K. (2006). Hippocampal vulnerability following traumatic brain injury: a potential role for neurotrophin-4/5 in pyramidal cell neuroprotection. Eur. J. Neurosci. 23,1089–1102.

Saatman, K.E., Contreras, P.C., Smith, D.H., Raghupathi, R., McDermott, K.L., Fernandez, S.C., Sanderson, K.L., Voddi, M., and McIntosh, T.K. (1997). Insulin-like growth factor-1 (IGF-1) improves both neurological motor and cognitive outcome following experimental brain injury. Exp. Neurol. 147,418–427.

Saatman, K.E., Duhaime, A.C., Bullock, R., Maas, A.I., Valadka, A., and Manley, G.T. (2008). Classification of traumatic brain injury for targeted therapies. J. Neurotrauma. 25,719–738.

Saatman, K.E., Feeko, K.J., Pape, R.L., and Raghupathi, R. (2006). Differential behavioral and histopathological responses to graded cortical impact injury in mice. J. Neurotrauma 23,1241–1253.

Saatman, K.E., Serbest, G., and Burkhardt, M.F. (2009). Axonal damage due to traumatic brain injury, in: *Vol. 15 Brain and Spinal Cord Trauma*. N. Banik, S. Ray (eds), *Handbook of Neurochemistry and Molecular Neurobiology*. Lajtha, A. (ed), Springer, NY: pps. 343–361.

Sandhir, R., and Berman, N.E. (2010). Age-dependent response of CCAAT/enhancer binding proteins following traumatic brain injury in mice. Neurochem. Int. 56,188–193.

Scheff, S.W., Baldwin, S.A., Brown, R.W., and Kraemer, P.J. (1997). Morris water maze deficits in rats following traumatic brain injury: lateral controlled cortical impact. J. Neurotrauma 14,615–627.

Scherbel, U., Raghupathi, R., Nakamura, M., Saatman, K.E., Trojanowski, J.Q., Neugebauer, E., Marino, M.W., and McIntosh, T.K. (1999). Differential acute and chronic responses of tumor necrosis factor-deficient mice to experimental brain injury. Proc. Natl. Acad. Sci. U.S.A. 96,8721–8726.

Schmued, L.C., Albertson, C., and Slikker, W. (1997). Fluoro-Jade: a novel fluorochrome for the sensitive and reliable histochemical localization of neuronal degeneration. Brain Res. 751,37–46.

Sheriff, F.E., Bridges, L.R., and Sivaloganathan, S. (1994). Early detection of axonal injury after human head trauma using immunocytochemistry for beta-amyloid precursor protein. Acta Neuropathol. 87,55–62.

Smith, D.H., Soares, H.D., Pierce, J.E.S., Perlman, K.G., Saatman, K.E., Meaney, D.F., Dixon, C.E., and McIntosh, T.K. (1995). A model of parasagittal controlled cortical impact in the mouse: cognitive and histopathologic effects. J. Neurotrauma 12,169–178.

Stone, J.R., Singleton, R.H., and Povlishock, J.T. (2000). Antibodies to the C-terminus of the beta-amyloid precursor protein (APP): a site specific marker for the detection of traumatic axonal injury. Brain Res. 871,288–302.

Sutton, R.L., Lescaudron, L., and Stein, D.G. (1993). Unilateral cortical contusion injury in the rat: vascular disruption and temporal development of cortical necrosis. J. Neurotrauma 10,135–149.

Thompson, S.N., Gibson, T.R., Thompson, B.M., Deng, Y., and Hall, E.D. (2006). Relationship of calpain-mediated proteolysis to the expression of axonal and synaptic plasticity markers following traumatic brain injury in mice. Exp. Neurol. 201,253–265.

Tsenter, J., Beni-Adani, L., Assaf, Y., Alexandrovich, A.G., Trembovler, V., and Shohami, E. (2008). Dynamic changes in the recovery after traumatic brain injury in mice: effect of injury severity on T2-weighted MRI abnormalities, and motor and cognitive functions. J. Neurotrauma 25,324–333.

Whalen, M.J., Dalkara, T., You, Z., Qiu, J., Bermpohl, D., Mehta, N., Suter, B., Bhide, P.G., Lo, E.H., Ericsson, M., and Moskowitz, M.A. (2008). Acute plasmalemma permeability and protracted clearance of injured cells after controlled cortical impact in mice. J. Cereb. Blood Flow Metab. 28,490–505.

Xiong, Y., Shie, F.S., Zhang, J., Lee, C.P., and Ho, Y.S. (2005). Prevention of mitochondrial dysfunction in post-traumatic mouse brain by superoxide dismutase. J Neurochem. 95,732–744.

You, Z., Savitz, S.I., Yang, J., Degterev, A., Yuan, J., Cuny, G.D., Moskowitz, M.A. and Whalen, M.J. (2008). Necrostatin-1 reduces histopathology and improves functional outcome after controlled cortical impact in mice. J. Cereb. Blood Flow Metab. 28,1564–1573.

Yu, S., Kaneko, Y., Bae, E., Stahl, C.E., Wang, Y., van Loveren, H., Sanberg, P.R., and Borlongan, C.V. (2009). Severity of controlled cortical impact traumatic brain injury in rats and mice dictates degree of behavioral deficits. Brain Res. 1287,157–163.

Address correspondence to:
Kathryn E. Saatman, Ph.D.
Spinal Cord and Brain Injury Research Center (SCoBIRC)
University of Kentucky
B473 Biomedical and Biological Sciences Research Building (BBSRB)
741 South Limestone Street
Lexington, KY 40536-0509

E-mail: k.saatman@uky.edu